UNIVERSITÉ DU LUXEMBOURG

Faculty of Science, Technology and Communication

Master in Integrated Systems Biology

MASTER thesis

by

Carole GOEBEL
Born on 18 March 1990 in Dudelange (Luxembourg)

Role of HIF-1α in Oncostatin M induced metabolic reprogramming of human hepatocytes

Defense: 15 July 2015 in Luxembourg

Supervisor(s): André Wegner, PhD, Luxembourg
Karsten Hiller, PhD, Luxembourg

This project was performed within the Metabolomics Group at the Luxembourg Centre for Systems Biomedicine (LCSB).

Supervisors:

André Wegner, PhD, Metabolomics Group at LCSB

Karsten Hiller, PhD, Metabolomics Group at LCSB

Reviewers:

Emilie Muller, PhD, Eco-Systems Biology Group at LCSB

Christelle Bahlawane, PhD, Molecular Disease Mechanisms Group at LSRU

Content

List of Figures

List of Tables

Abstract

Hypoxia and inflammation have been associated with carcinogenesis. Both microenvironments induce alterations in central carbon metabolism, leading to a more cancerous metabolic phenotype. Even in the presence of oxygen, many cancer cells adapt their cellular metabolism towards a hypoxia-like metabolic phenotype, including increased glucose uptake, higher glycolytic flux, increased lactate production, and decreased O_2 consumption, a phenomenon known as Warburg effect. In part this response is mediated by hypoxia inducible factor-1α (HIF-1α), a transcriptional key regulator of the cellular response to hypoxia. Using stable isotope assisted metabolomics, I investigated the role of HIF-1α in oncostatin M (OSM) mediated metabolic reprogramming of the human hepatocyte cell line PH5CH8. I show that under normoxia, OSM-induced up-regulation of HIF-1α results in a hypoxia-like metabolic phenotype. Although, glucose uptake and lactate secretion are only slightly increased, stable isotope labelling revealed drastic changes in intracellular metabolic fluxes. In particular, I show that OSM suppresses glucose and glutamine oxidation in the tricarboxylic acid cycle via pyruvate dehydrogenase kinase 1 (PDK1) mediated inhibition of pyruvate dehydrogenase. This finding highlights the role of PDK1 as one of the key enzymes, responsible for the OSM-induced metabolic phenotype. As a result of the impaired glucose oxidation, PH5CH8 show higher rates of reductive glutamine metabolism.

Finally, I demonstrate that HIF-1α is critical for OSM-mediated metabolic reprogramming. Silencing *HIF-1α* almost completely impeded OSM-induced metabolic changes, connecting HIF-1α, inflammation, and cancer cell metabolism.

Altogether, the results obtained in this thesis might provide a causal link between chronic inflammation and malignant cellular transformation.

Abbreviations

2-OG	2-oxoglutarate
α-KG	α-ketoglutarate
Asn	Asparagine
BCAA	Branched chain amino acid
bHLH/ PAS	Basic helix-loop-helix-PER/ARNT/SIM
BSA	Bovine serum albumin
Cit	Citrate
CNTF	Ciliary neutrophic factor
CSF	Cerebrospinal fluid
CT-1	Cardiotrophin-1
DPBS	Dulbecco's Phosphate Buffered Saline
dFBS	Dialyzed fetal bovine serum
dNTP	Deoxyribonucleotide triphosphate
EGF	Epidermial growth factor
EPO	Erythropoietin
FA	Fatty acids
FIH	Factor inhibiting HIF
G-CSF	Granulocyte-colony stimulating factor
GC-MS	Gas chromatography coupled to mass spectrometry
GLUT1/3	Glucose transporter 1/3
GM-CSF	Granulocyte macrophage-colony stimulating factor
gp130	Glycoprotein 130
HCC	Hepatocellular carcinoma
HIF-1	Hypoxia inducible factor-1
HK1	Hexokinase 1
HPLC	High-pressure liquid chromatography
HRE	Hypoxia-response element
IDH	Isocitrate dehydrogenase
IL-6	Interleukin 6
Jak	Janus kinase
L27	Housekeeping gene
Lac	Lactate
LDH	Lactate dehydrogenase
LIF	Leukemia inhibitory factor
M-CSF	Macrophage-colony stimulating factor
MAPK	Mitogen-activated protein kinase
MID	Mass isotopomer distribution
MOX	Methoxyamine hydrochloride
MSTFA	N-Methyl-N-(trimethylsilyl)-trifluoracetamide
MTBSTFA	N-(tert-butyldimethylsilyl)-N-methyltrifluoroacetamide
ODDD	Oxygen dependent degradation domain
OSM	Oncostatin M
PAI1	Plasminogen activator inhibitor 1
PC	Pyruvate carboxylase
PDH	Pyruvate dehydrogenase
PDK1	Pyruvate dehydrogenase kinase 1
PEP	Phosphoenolpyruvate
PGK1	Phosphoglycerate kinase 1
PHD	Prolyl 4-hydroxylase domain proteins
PI3K	Phosphatidylinositol-3-kinase
PK	Pyruvate kinase
PKM2	Pyruvate kinase isomer M2

Pro	Proline
qPCR	Real-time polymerase chain reaction
S/SL	Split/splitless inlet
SDH	Succinate dehydrogenase
SIM	Single ion monitoring mode
SRC-1	Steroid receptor coactivator-1
STAT3	Signal transducers and activators of transcription 3
TBDMS	Tert-butyldimethylsilyl
TBS-T	Tris-buffered saline – tween
TCA cycle	tricarboxylic acid cycle
TGFα	Tumor growth factor
TMS	Trimethylsilyl
VEGF	Vascular endothelial growth factor
VHL	Von Hippel Lindau tumor suppressor protein

1 Introduction

1.1 Biological background

1.1.1 Hepatocellular carcinoma

Liver cancer is the sixth most common cancer and the third cause of cancer-related death worldwide (1). Over 90% of primary liver cancers are hepatocellular carcinomas (HCC) (1). HCC development can be the consequence of liver cirrhosis caused by alcoholic liver disease, non-alcoholic fatty liver disease (hepatosteatosis), or aflatoxin exposure (*Aspergillus flavus*) (1). Most HCCs are preceded by chronic inflammation due to viral hepatitis infections (hepatitis B and C virus), suggesting that an inflammatory microenvironment promotes HCC development (1). Prominent mediators of this immune response are interleukin (IL)-6-type cytokines. Besides their regulatory role in chronic inflammation and immune response, IL-6-type cytokines are key players in the regulation of cancer development and progression (2).

1.1.2 IL-6-type cytokine signalling

The family of IL-6-type cytokines includes IL-6, interleukin-11 (IL-11), oncostatin M (OSM), ciliary neurotrophic factor (CNTF), leukemia inhibitory factor (LIF), cardiotrophin-1 (CT-1), and cardiotrophin-like cytokine (CLC) (3). IL-6-type cytokines activate target genes involved in cell differentiation, survival, apoptosis, and proliferation (3). They initiate the Janus kinase/ Signal transducer and activator of transcription 3 (JAK/STAT3) signalling cascade. Ligand-binding induces membrane receptor homo- or heterodimerization. The dimeric receptors are composed of a gp130 and a ligand specific subunit (4), including non-signalling α-receptors (IL-6-receptor α, IL-11-receptor α, and CNTF receptor α) or signal transducing receptors (gp130, LIF-receptor, and OSM-receptor) (3,4).

Upon ligand binding, activated JAKs bind the membrane-proximal region of the dimeric cytokine receptor, leading to phosphorylation at tyrosine residues (3,4). Cytokine receptor phosphorylation results in the activation of multiple major signalling pathways, including STAT3, phosphatidylinositol-3-kinase (PI3K)/Akt(5), and the mitogen-activated protein kinases (MAPK) pathway (3,4). All IL-6-type cytokines induce STAT3 by the following activation mechanism: monomeric STAT3 is recruited to the activated IL-6-type cytokine receptor (3) where it binds to the phosphotyrosine sites via the src homology (SH)-2 domain, resulting in tyrosine phosphorylation on the C-terminal domain of STAT3. The SH-2 domain of one active STAT3 monomer and the phosphotyrosine of the other active monomer interact

and form a dimer. As a consequence of dimerization, the STAT3 homodimer translocates into the nucleus where it binds to transcription factor binding sides of genes involved in cell survival and proliferation (3,4,6). Figure 1.1 depicts the OSM-mediated STAT3 signalling pathway as an example of IL-6 type cytokine signalling.

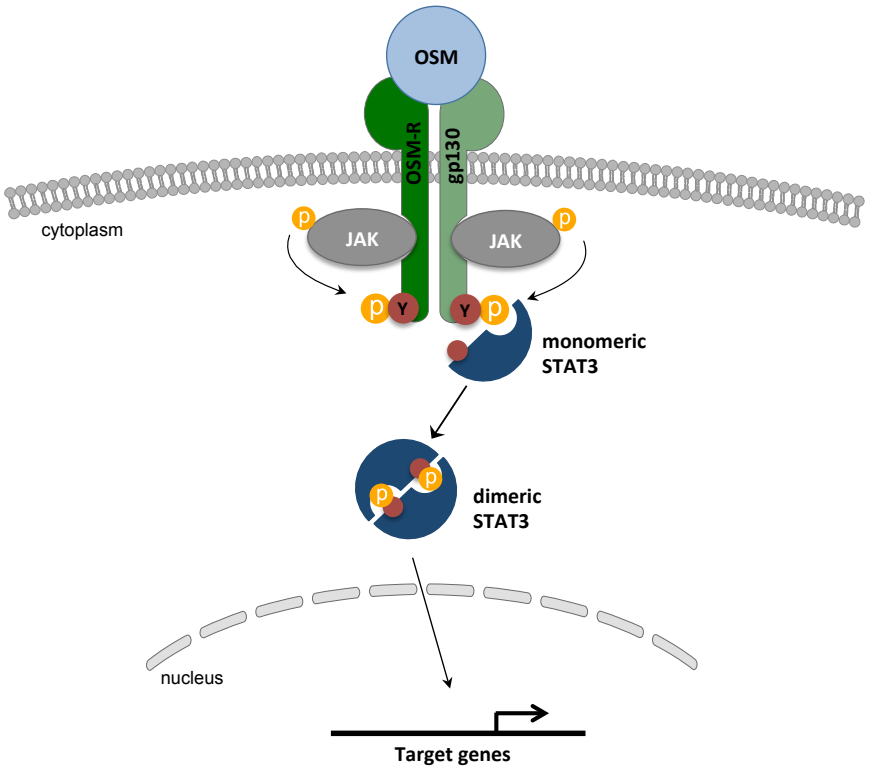

Figure 1.1 OSM activates the JAK/STAT pathway. OSM binds to the LIF-receptor or to the OSM-receptor associated to a gp130 monomer. Upon ligand binding, the OSM-R and gp130 dimerize. Subsequently, JAKs are activated and bind to the cytokine receptor, leading to its phosphorylation, which in turn activates signal transducers and activators of transcription 3 (STAT3). The SH-2 domain of one active STAT3 monomer and the phosphotyrosine of the other active monomer interact and form a dimer. The STAT3 homodimer translocates into the nucleus where it binds to responsive elements on gene promoters.

1.1.3 STAT3 signalling

The pro-oncogenic transcription factor STAT3 exerts a central role in pro-inflammatory signalling downstream of IL-6-type cytokine stimulation (7). Aberrant STAT3 activation is commonly observed in human cancers, including leukemia's, lymphomas, lung, gastric, hepatocellular, colorectal, and prostate cancer (6) and consists a point of convergence between pro-inflammatory signalling and cancer development (7). Constitutively activated

STAT3 plays an important role in tumour-promoting inflammation and regulates numerous genes involved in cancer cell progression, proliferation (e.g. c-myc, cyclin D1), invasion (matrix metalloproteinase-2), cell survival (e.g. survivin, bcl-xl, myeloid cell leukemia-1, B-cell lymphoma-2 and cIAP2) and angiogenesis (vascular endothelial growth factor (VEGF)) (7). Beside IL-6-type cytokines, growth factors (e.g. TGFα, EGF, G-CSF, M-CSF or GM-CSF), oncogenic proteins, carcinogens (e.g. cigarette smoke) and environmental stress can activate the STAT3 signalling cascade (6).

Recently, it was shown that the IL-6-type cytokine OSM induces the expression of hypoxia inducible factor-1α (*HIF-1α*) in immortalized hepatocytes and hepatocellular carcinoma cells (8). Vollmer and colleagues showed that *HIF-1α* mRNA and HIF-1α protein levels are upregulated under normoxic *in vitro* conditions (21% O_2) in response to the OSM mediated STAT3 activation (8). In contrast to hypoxia, OSM signalling does not contribute to an increased HIF-1α stability, but solely enhances *HIF-1α* expression (8).

1.1.4 Regulation of HIF

HIFs, including HIF-1,-2, and -3, are part of the basic helix-loop-helix-PAS (bHLH/ PAS) (9,10) family of transcription factors and are primarily regulated post-translationally (11). HIF-1 is a heterodimer that consists of two subunits, the constitutively expressed HIF-1β subunit and the O_2-dependant HIF-1α subunit (11). As the key regulator of the cellular response to low oxygen levels, HIF-1 is essential for cell survival under hypoxic conditions (9). The HIF-1α subunit is stabilized under hypoxic conditions whereas it is continuously degraded in a normoxic environment.

HIF-1α is constitutively expressed but its stability is negatively regulated by O_2-dependent prolyl 4-hydroxylase domain proteins (PHD) (Figure 1.2). Under normal oxygen tensions, PHD hydroxylates the two conserved proline residues Pro402 and Pro564 within the oxygen dependent degradation domain (ODDD) of HIF-1α. This hydroxylation reaction depends on the availability of molecular oxygen (O_2), 2-oxoglutarate (2-OG), as well as iron (Fe^{2+}) and ascorbate (12). Subsequently the von Hippel Lindau tumour suppressor protein (VHL) binds the hydroxylated prolines residues leading to HIF-1α polyubiquitination and proteasome-mediated degradation (9) (Figure 1.2). Degradation of HIF-1α is extremely rapid with a half-life of less than 5 minutes. However, under hypoxic conditions the activity of PHD, due to lack of O_2, is suppressed and HIF-1α is stabilized (11).

Under normoxic condition, the transcriptional activity of HIF-1α is regulated by the factor inhibiting HIF (FIH) which hydroxylates the asparagine residue 803 (Asn803) and thereby inhibits the binding of the transcriptional co-activator p300/CBP. HIF-1α can be stabilized and active under normoxic conditions. The TCA cycle intermediates succinate and fumarate have been reported to increase HIF-1α stability by inhibiting PHD activity. Both intermediates bind

to the 2-OG- or Fe^{2+}-binding sites of PHD, thereby blocking the interaction with proline in the ODDD of HIF-1α (12). Mutations in the succinate dehydrogenase (SDH) result in an accumulation of succinate, inhibiting PHD in the cytosol (12). Furthermore, it has been shown that in renal cell carcinoma and congenital erythrocytosis, mutations in VHL and PHD lead to an up-regulation of HIF-1α (13).

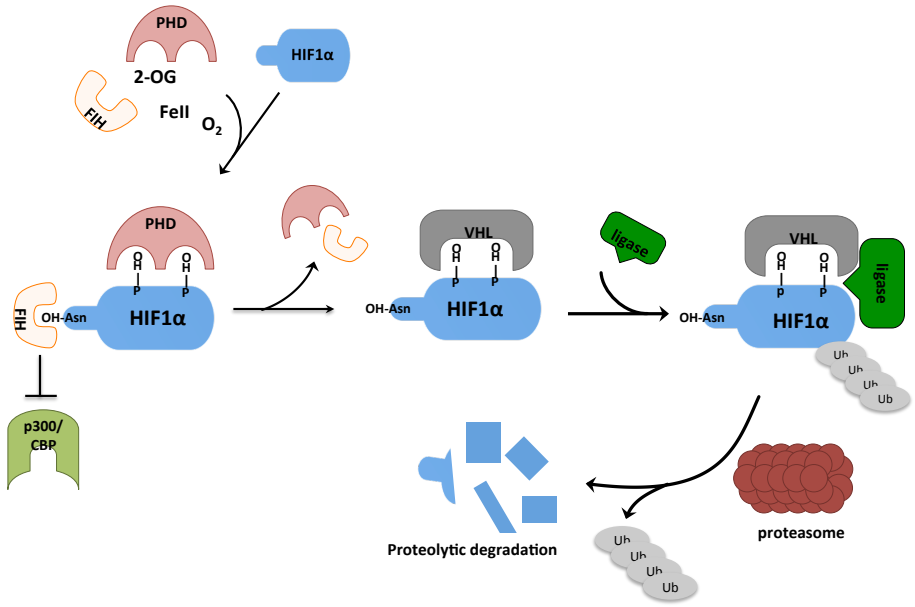

Figure 1.2 HIF-1α regulation under normoxic conditions. In normoxia HIF-1α is hydroxylated by PHD in the presence of O_2, Fe^{2+}, 2-oxoglutarate (2-OG), and ascorbate. FIH hydroxylates the asparagine residue to inhibit the binding of the transcriptional co-activator p300/CBP. Hydroxylated HIF-1α is recognized by von VHL protein together with ubiquitin ligase complex, leading to its polyubiquitination and targeting it for proteasome-mediated degradation.

Once HIF-1α is stabilized, it translocates to the nucleus where HIF-1α and HIF-1β form a heterodimer and recruit other transcriptional co-activators such as p300/CBP histone acetyltransferase, steroid receptor coactivator-1 (SRC-1) family or nuclear redox regulator (Ref-1). The HIF-1-p300/CBP complex recognizes the consensus nucleotide sequence 5'-RCGTG-3' of hypoxia-response elements (HREs) within the promoter regions of numerous target genes (10,14) and promotes their transcription. HIF-1α activates the transcription of genes encoding for the vascular endothelial growth factor (VEGF), plasminogen activator inhibitor 1 (PAI1), which are crucial for angiogenesis and tissue remodelling, and erythropoietin (EPO), involved in erythropoiesis. Moreover, HIF-1α regulates the expression of numerous genes involved in the adaptation of the cellular metabolism to low oxygen

tensions (15). Figure 1.3 gives an overview of the nuclear translocation, heterodimerization and lists the important HIF-1α target genes.

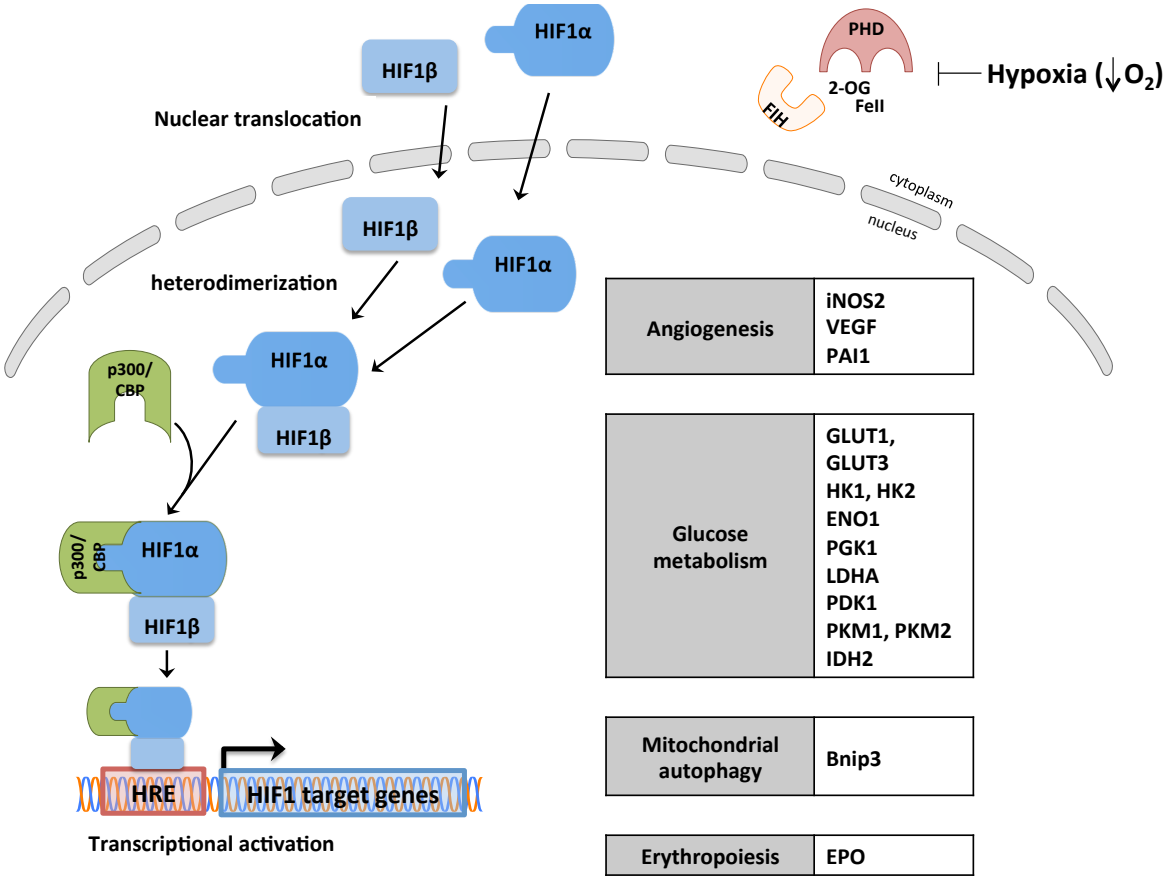

Figure 1.3 HIF-1α regulation in response to hypoxia. Under hypoxic conditions, proline and asparagine hydroxylations are inhibited. VHL cannot bind and target HIF-1α for proteasomal degradation, which leads to HIF-1α accumulation and translocation to the nucleus. The constitutively expressed HIF-1β subunit translocates to the nucleus to form a heterodimer with HIF-1α, which recruits other transcriptional co-activators such as p300/CBP. The complex binds to HREs within the promoters of target genes involved in angiogenesis, glucose metabolism mitochondrial autophagy and erythropoiesis.

1.1.5 Effects of HIF-1α on cellular metabolism

HIF-1α is indispensable to adapt cellular metabolism to hypoxic environments. It is well established that HIF-1α orchestrates the expression of several genes that drives the change from oxidative phosphorylation towards a more glycolytic metabolic phenotype (10) (Figure 1.3). HIF-1α regulates the expression of glucose transporters (e.g., *GLUT1* and *GLUT3*) to increase glucose import into the cytoplasm and promotes higher rates of glycolysis by up-regulating glycolytic genes, including lactate dehydrogenase A (*LDHA*), phosphoglycerate

kinase 1 (*PGK1*) and hexokinase 1 (*HK1*), promoting high rates of glycolysis (Figure 1.4). HIF-1α indirectly reduces mitochondrial pyruvate oxidation through the up-regulation of pyruvate dehydrogenase kinase 1 (PDK1). In turn, PDK1 phosphorylates and inactivates pyruvate dehydrogenase complex (PDH), which oxidizes pyruvate to acetyl-CoA (Figure 1.5). As a result the entry of pyruvate into the TCA cycle is diminished, leading to reduced mitochondrial oxidative phosphorylation. As a result of increased glycolysis, increased LDH and reduced PDH activity, the glycolytic flux is deviated and pyruvate is converted to lactate (10,16,17).

As a consequence of reduced PDH activity under hypoxic conditions, citrate production from glucose-derived acetyl-CoA is drastically reduced. However, citrate is an important metabolite required to transport acetyl-CoA moieties from mitochondria to the cytosol, where it is an important precursor for fatty acid synthesis and protein acetylation (18). As the citrate pool is drastically reduced under hypoxic conditions, the cellular metabolism needs to be adapted in order to ensure proliferation and growth (10).

Besides glucose, the amino acid glutamine is required as a major carbon source in eukaryotic cells. At normal oxygen tension, glutamine is required to support cell growth and division (19,20). Glutaminase catalyses the conversion of glutamine to glutamate, which is converted to α-ketoglutarate via glutamate dehydrogenase. Thereby, glutamine-derived α-ketoglutarate can be oxidatively or reductively metabolized in the TCA cycle (Figure 1.5). In oxidative glutamine metabolism, α-ketoglutarate is oxidized to succinate and eventually converted to citrate in the TCA cycle. This includes citrate synthase, which condenses acetyl-CoA and oxaloacetate to citrate.

Since citrate production from glucose-derived acetyl-CoA is drastically reduced in hypoxic conditions, citrate can also be generated from isocitrate by aconitase (Figure 1.5). Therefore, isocitrate is produced from α-ketoglutarate, catalysed by isocitrate dehydrogenase (IDH). The reaction of IDH is reversible and leads to the possibility of citrate generation from glutamine-derived α-ketoglutarate, without the necessity of free acetyl-CoA (Figure 1.5). For that, glutamine-derived α-ketoglutarate is reductively carboxylated to isocitrate by IDH and eventually converted to citrate. Conditions lowering mitochondrial citrate levels such as hypoxia or complex 1 inhibition have been shown to increase reductive α-ketoglutarate carboxylation by mass action (19). This metabolic flux is of critical importance for lipid synthesis, when acetyl-CoA availability becomes scarce (19,21).

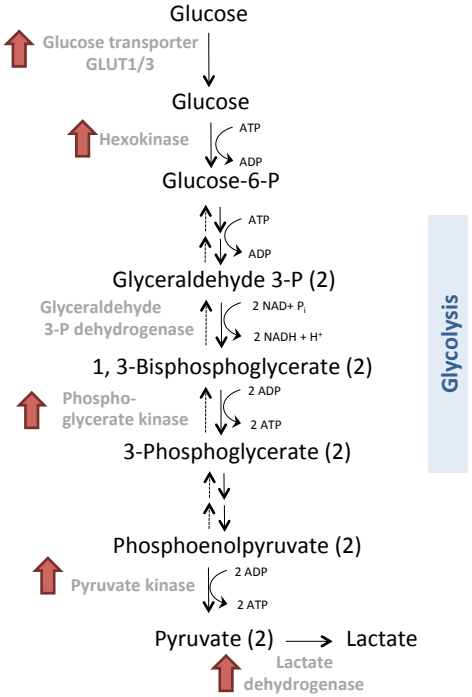

Figure 1.4 Simplified scheme of the glycolysis. Metabolites are shown in black, enzymes in grey. Glucose is transported to cells by glucose transporters (GLUT). Pyruvate is the end product of glycolysis and can be converted either to acetyl- CoA or lactate via lactate dehydrogenase. In hypoxia several glycolytic enzymes are up-regulated, represented by the red arrows (22).

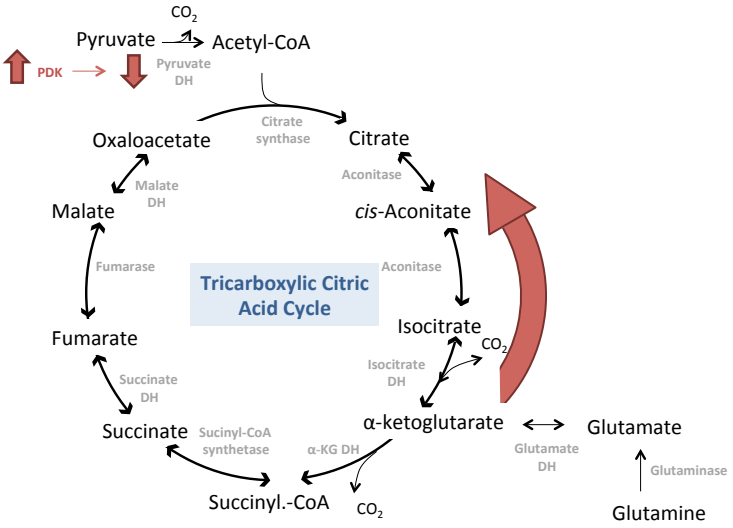

Figure 1.5 Simplified scheme of tricarboxylic citric acid cycle (TCA). Metabolites are shown in black, enzymes in grey. In hypoxia, PDH is inhibited and the reductive glutamine metabolism is enhanced (22).

Enhanced glycolysis and lactate production in cancer and highly proliferating cells imply an increased conversion of phosphoenolpyruvate (PEP) and ADP to pyruvate and ATP by pyruvate kinase (PK) (Figure 1.4). Recent studies revealed that HIF-1α activates the transcription of the alternative splicing variant pyruvate kinase isomer M2 (*PKM2*). Yang and co-workers identified PKM2 as a protein kinase critical for the Warburg effect and tumorigenesis. Monomeric PKM2 translocates to the nucleus where it functions as a protein kinase that phosphorylates histone H3. Consequently PKM2 activates the transcription of *CCND1* (encoding for cyclin D1) and *MYC* (23). Cyclin D1 mediates cell cycle progression and c-Myc in turn, up-regulates the expression of the glycolytic enzymes *GLUT1* and *LDHA*, increasing glucose uptake and lactate production respectively (23). Furthermore PKM2 functions as a transcriptional coactivator of HIF-1α thereby activating the transcription of numerous target genes, including *GLUT1*, *LDHA* and *PDK1* (23–25). Recently, PKM2 has also been shown to promote the Warburg effect in lipopolysaccharide-induced macrophages (25).

1.1.6 Cellular metabolism: connecting inflammation and carcinogenesis?

Hypoxic and inflammatory conditions have been associated with carcinogenesis (26,27) and associated with high glycolytic rates (10,26). Regardless of the oxygen supply many cancer cells shift their metabolism towards a hypoxia-like metabolic phenotype including increased glucose uptake, glycolytic flux, lactate production, and decreased O_2 consumption. This phenomenon is known as the Warburg effect (20). It is assumed that this metabolic adaptation enables cancer cells to synthesize essential macromolecules (e.g., nucleotides, amino acids, and lipids) required for survival, rapid proliferation, and growth. For example, high glucose turnover provides necessary intermediates such as ribose-5-phosphate, serine and glycine for amino acid and nucleotide synthesis (20). OSM-mediated HIF-1α up-regulation provides a link between metabolic adaptations to low oxygen tension and cancer cell metabolism. Therefore, OSM-induced HIF-1α up-regulation might connect chronic inflammation and malignant cellular transformation. IL-6-type cytokine induced STAT3 signalling plays an important role in the regulation of many processes involved in immune response of tumour cells, angiogenesis, and hematopoiesis. These processes are often linked to an hypoxic environment with HIF-1α as important regulator. Thereby HIF-1α regulates the expression of many genes involved in angiogenesis, hematopoiesis and central carbon metabolism. However, it is still debated whether the metabolic changes are a consequence or a cause of carcinogenesis (28).

1.2 Technical background

1.2.1 Metabolomics

Metabolomics is the study of global metabolite profiles in a biological system at a given time under a defined set of conditions. It investigates intracellular and extracellular metabolites in biological samples, including cells grown in culture, tissue, or biological fluids (e.g. plasma, urine, cerebrospinal fluid). Compared to the other three big “omics”; genomics, proteomics, and transcriptomics, metabolomics offers unique advantages. For example, gene expression does not necessarily correlate with protein levels and protein activity might be regulated on a posttranscriptional level. Metabolites, however, reflect the end point of all those regulatory processes and, therefore, provide a much closer functional link to an observed phenotype.

However, the metabolome is much more chemically diverse as for example the genome or proteome, which makes the metabolome analysis and interpretation of metabolome data challenging. To aid interpretation, metabolome analysis should, therefore, be combined with e.g, molecular biology techniques such as Western blot assay or real-time polymerase chain reaction (qPCR).

Generally a metabolomics experiments can be divided into three main steps: sample preparation, analytical mass spectrometric measurements and computational data analysis (29–31).

1.2.2 Sample preparation

As the turnover rate of metabolites lies in the range of seconds, sample preparation requires an efficient quenching and metabolite extraction procedure. Quenching methods use low temperature and organic solvents to denature the tertiary structure of proteins and prevent active metabolic enzymes to change in the metabolic state. The protocols, developed for quenching and extraction of metabolites depend on the type of biological sample, the targeted metabolites (e.g. non-polar or polar metabolites) and the analytical technique (32,33). In this thesis, I used ice-cold methanol-water-chloroform extraction method resulting in the separation of three component phases: the upper polar methanol-water phase containing polar metabolites, the lower non-polar chloroform phase containing non-polar metabolites and the interphase containing total RNA, DNA and proteins.

1.2.3 Gas chromatography coupled to mass spectrometry (GC-MS)

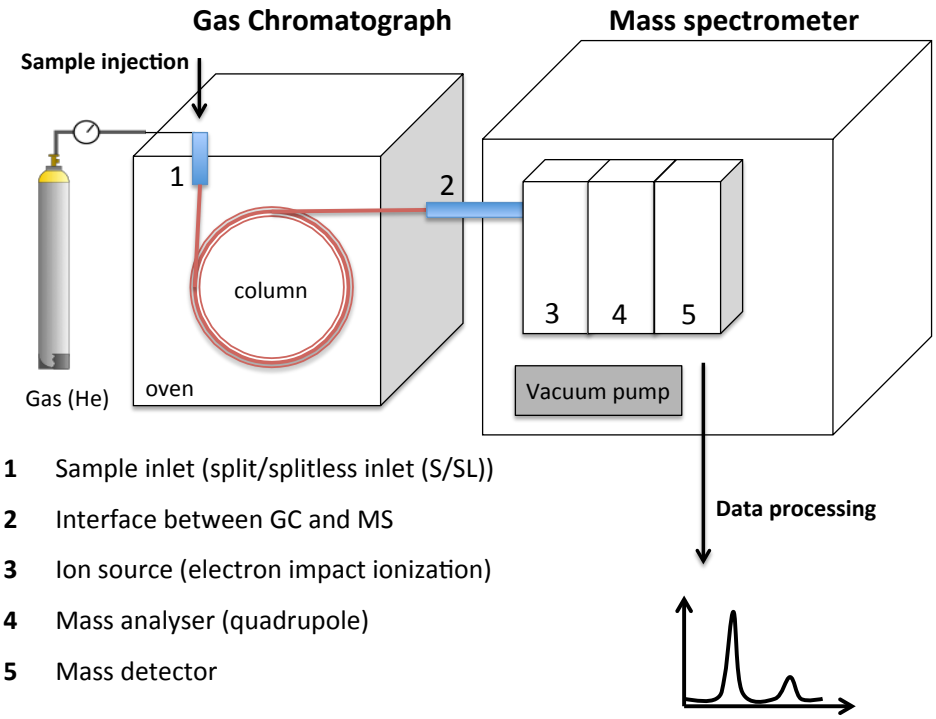

Figure 1.6 GC-MS scheme. The samples are injected into the sample inlet and are separated by gas chromatography. Through the interface the separated compounds are processed in the mass spectrometer and their mass to charge ratio is detected. The mass spectrometer is composed of three blocks: an ion source, a quadrupole mass analyser, and a mass detector.

Metabolite levels can be assessed by mass spectrometry coupled to a chromatographic separation technique such as gas chromatography. The GC-MS is composed of a GC and a MS building block (Figure 1.6). The first building block separates metabolites from a complex mixture by GC. Since the GC operates in a gas phase, only volatile compounds can be separated[37]. For that reason, polar carbonyl, carboxyl, and amine groups must chemically be modified prior to analysis. Methoxyamine hydrochloride is used to mask the carbonyl groups. In addition, N-Methyl-N-(trimethylsilyl)-trifluoracetamide (MSTFA) or N-(tert-butyldimethylsilyl)-N-methyltrifluoroacetamide (MTBSTFA) mask the carboxyl, hydroxyl, amine, and amide groups (Figure 1.7). The resulting chemical derivatives, trimethylsilyl (TMS) derivatives or tert-butyldimethylsilyl (TBDMS) are less polar, more volatile and more stable at high temperature than their precursors (34).

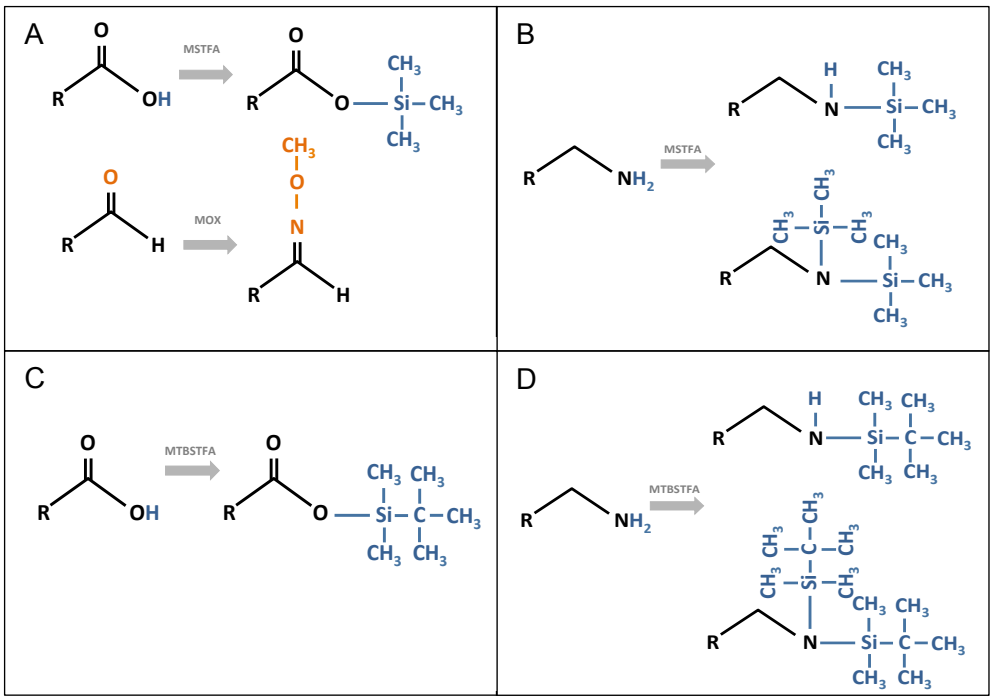

Figure 1.7 Chemical derivatization for GC-MS measurement. Hydrogen atoms of polar groups are derivatized by MSTFA and MTBSTFA, shown in blue. Carbonyl groups are derivatized by methoxyamine hydrochloride (MOX), shown in orange. The resulting TMS or TBDMS derivatives are more volatile and more stable at high temperature than their precursors.

After the compounds are separated in the GC, they are ionized in the mass spectrometer. The most common ionization method used in GC-MS is electron impact ionization (EI), because EI ionization creates reproducible fragmentation patterns. Subsequently to ionization, the mass detector detects the mass to charge ratio (m/z) of these fragment ions. The resulting mass spectrum consists of numerous different fragment ions, also called isotope clusters (Figure 1.8) (35). Each isotope cluster is composed of multiple peaks because of naturally occurring stable isotopes (e.g. ^{12}C and ^{13}C for carbon or ^{16}O and ^{18}O for oxygen). A two-carbon compound creates mass spectra with three peaks, where the first major peak generally represents the monoisotopoic peak M+0. The low abundance peaks represent all combinations of the naturally abundant isotopes, usually corresponding to the compound with one mass unit above the monoisotopic peak M+1 (one ^{12}C atom is replaced by ^{13}C) or two mass unit above the monoisotopic peak M+2, if both ^{12}C atoms are substituted by ^{13}C. Each peak of the isotope cluster corresponds to the identical structural compound but different isotopic composition.

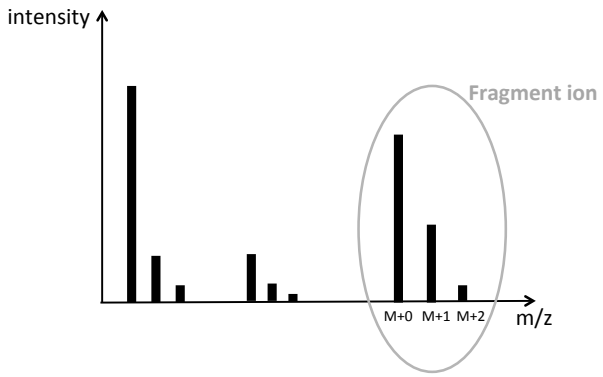

Figure 1.8 GC-MS mass spectrum. Typically a mass spectrum is composed of different fragment ions. Each fragment ion is associated to an isotope cluster. The monoisotopoic peak denoted as M+0 results from the combination of the lightest isotopes of all elements (e.g. ^{12}C, ^{1}H, ^{16}O). The other peaks represent combinations of the naturally abundant isotopes, e.g. compounds with one mass unit above the monoisotopic peak are denoted M+1 and compounds with two mass units above the monoisotopic peak as M+2.

1.2.4 Stable isotope assisted metabolomics

Metabolomics provides the means to analyse metabolite levels and to detect changes thereof in response to different external perturbations. This might be sufficient to detect biomarkers, but in certain cases fails to detect intracellular flux changes. For example the abundance of citrate in the TCA cycle can be assessed for a given set of conditions. However, the level of citrate does not allow discerning between the PC pathway and PDH (Figure 1.9). In this example, pyruvate can be metabolized either to acetyl-CoA and eventually to citrate by PDH, or to oxaloacetate through PC, which is then converted to citrate.

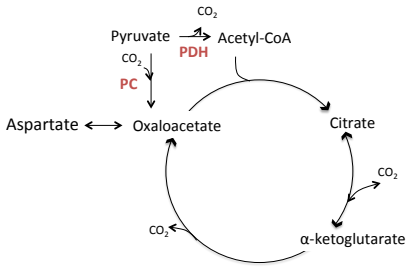

Figure 1.9 Simplified scheme of the tricarboxylic citric acid cycle. Either Pyruvate is carboxylated into oxaloacetate via PC or metabolized into acetyl-CoA by PDH. Acetyl-CoA enters the TCA cycle and is oxidatively decarboxylated to citrate.

To obtain information about intracellular fluxes, stable isotope assisted metabolomics can be applied. For that stable isotope labelled compounds are added to the cell culture. Beside deuterium (^{2}H) and nitrogen (^{15}N), carbon (^{13}C) labelled compounds are used for stable isotope assisted metabolomics experiments. To profile central carbon metabolism, [U-$^{13}C_6$]glucose or [U-$^{13}C_5$]glutamine are most commonly applied. Based on the enzyme activities within a cell, the isotopically labelled compounds are distributed within the metabolic network, affecting the molecular weight of pathway intermediates. These mass differences can be detected with GC-MS. Figure 1.10 depicts an example how stable isotopes can be used to differentiate between PC and PDH activity using uniformly labelled pyruvate as a tracer ([U-$^{13}C_3$]pyruvate). Depending on the respective pathway activity, carbon bonds of pyruvate are broken and rearranged specifically. If pyruvate is metabolized via PDH, two carbon atoms of citrate are pyruvate derived, leading to [$^{13}C_2$]citrate, whereas three carbons are pyruvate-derived when pyruvate is carboxylated by PC, leading to [$^{13}C_3$]citrate (36,37).

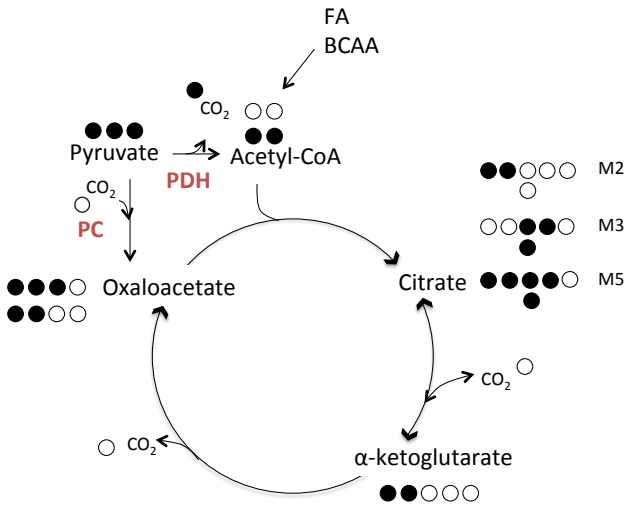

Figure 1.10 Simplified scheme of the TCA cycle. The carbon backbones of every metabolite are shown in circles. The black circles represent the ^{13}C and can be used as indicator for the flux via PDH, while the blue circles represent ^{13}C derived from carboxylation via PC. [$^{13}C_2$]citrate is produced through PDH and [$^{13}C_3$]citrate is produced from [$^{13}C_3$]oxaloacetate and unlabelled acetyl-CoA through PC.

1.2.5 Mass isotopomer distribution (MID)

Isotopic enrichment is usually quantified in form of MIDs, which describe the fractional abundance of each mass isotopomer of a particular compound. Mass isotopomers have the same structure but differ in the isotopic composition (Figure 1.11). More formally, mass isotopomers are groups of isotopologues of the same nominal mass (36). For example, pyruvate has four different mass isotopomers referred to as M0, M1, M2, and M3; unlabelled

pyruvate (M0), [$^{13}C_1$]pyruvate (M1), [$^{13}C_2$]pyruvate (M2), and uniformly labelled [$^{13}C_3$]pyruvate (M3).

Based on a mass spectrometric measurement, MIDs can be determined by solving the linear equation system $A \cdot f = I$, where A is the correction matrix to correct for natural occurring isotopes, f is the vector of the fractional abundances of each mass isotopomer and I is the vector of the measured mass spectral intensities (32) (Figure 1.11). In the example of a two-carbon compound (Figure 1.11), the first column of A contains the natural mass isotopomer distribution of the unlabelled compound ($M0_0$, $M0_1$ and $M0_2$). The second and third columns represent the natural mass isotopomer distribution if one of the carbon atoms is replaced by a ^{13}C ($M1_0$, $M1_1$ and $M1_2$) or both carbon atoms are replaced with a ^{13}C ($M2_0$, $M2_1$ and $M2_2$), respectively (Figure 1.12).

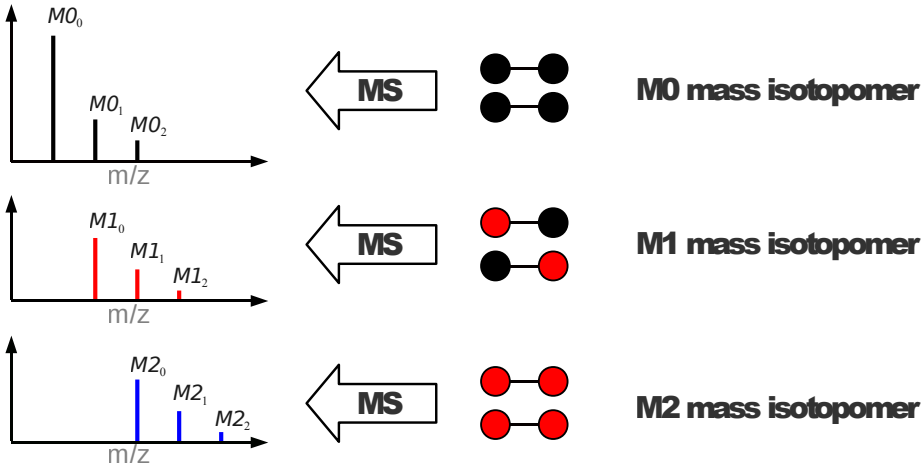

Figure 1.11 Mass isotopomer distribution of a two-carbon compound. Based on the number and position of incorporated labelled atoms, different isotopomers are shown (^{12}C in black, ^{13}C in red). The mass spectrum is depicted along with the corresponding mass isotopomer (figure based on Karsten Hiller *et al*., 2012).

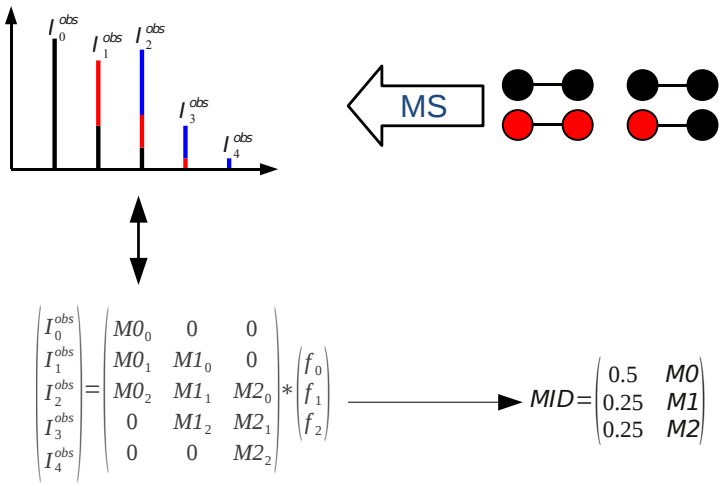

Figure 1.12 Mass isotopomer distribution and correction matrix. The mass spectrum is measured for a complex mixture of mass isotopomers and the fraction of each mass isotopomer (f) is determined by solving the linear equation system. In this case 50% of the molecules are unlabelled, 25% contain one stable isotope and 25% contain two stable isotopes (figure based on Karsten Hiller *et al*., 2012).

MIDs provide the means to reveal intracellular flux changes. The importance of MIDs can be best explained with a short example (Figure 1.13A): using the same example as in Figure 1.10 the MID of citrate provides direct information about the metabolic flux of pyruvate through PC and PDH using [$^{13}C_3$]pyruvate as a tracer. From the M2 and M3 mass isotopomers of citrate, the activity of the two pathways can be distinguished. If PDH is active, acetyl-CoA contains two ^{13}C atoms and in consequence M2 citrate is produced. In contrast, M3 citrate is produced when pyruvate is carboxylated via PC to [$^{13}C_3$]oxaloacetate (Figure 1.13B). The ratio of M2 to M3 citrate then provides information about relative activity of PDH to PC.

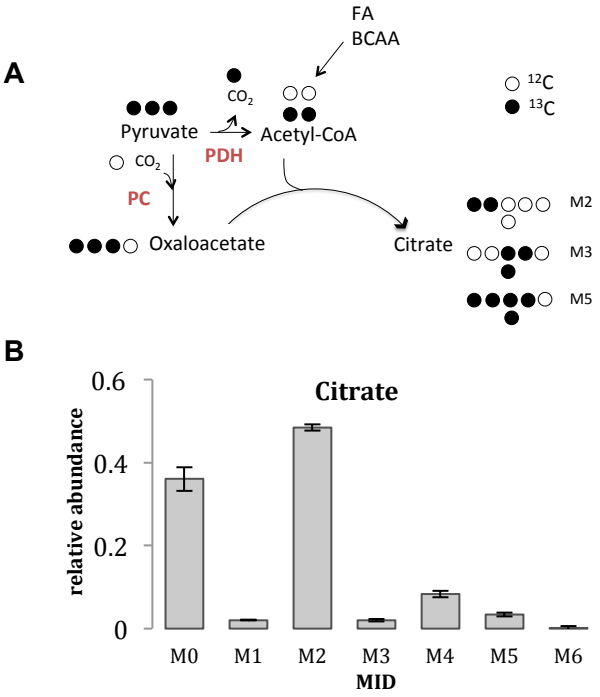

Figure 1.13 Mass isotopomer distribution of citrate. (A) Simplified scheme of pyruvate dehydrogenase and pyruvate carboxylase pathway. The carbon backbones of every metabolite are shown in circles. The black circles represent ^{13}C, while the white circles represent ^{12}C. Using uniformly labelled pyruvate as a tracer, PDH activity generates acetyl-CoA containing two ^{13}C atoms and produces M2 citrate, whereas PC activity generates M3 citrate via [$^{13}C_3$]oxaloacetate. (B) The relative isotope abundance of each mass isotopomer (M0, M1, M2, M3, M4, M5 and M6) of citrate is shown. Most of the citrate contains two ^{13}C atoms (0.55% M2), suggesting that pyruvate is metabolized mostly via PDH pathway.

1.3 Aim of thesis

Based on the previous finding that *HIF-1α* mRNA and HIF-1α protein levels are significantly increased in response to OSM mediated STAT3 signalling under normoxic conditions (Vollmer *et al*., 2009) (8), the purpose of this master's thesis was to investigate the effects of OSM-induced HIF-1α up-regulation on central carbon metabolism in the immortalized hepatocyte cell line PH5CH8. OSM mediated HIF-1α up-regulation provides a common link between the metabolic adaptations to low oxygen tension and cancer cell metabolism, and therefore, might provide a causal link between chronic inflammation and malignant cellular transformation. For that reason, I investigated whether OSM-dependent HIF-1α up-regulation at normal oxygen tension results in a hypoxia like metabolic phenotype in immortalized hepatocytes and whether this provides a link between inflammation and malignant cellular transformation. To highlight the role of HIF-1α, I studied the effect of OSM stimulation and *HIF-1α* silencing in normoxic (21% O_2) and hypoxic conditions (1% O_2) respectively using stable isotope assisted metabolomics and molecular biology techniques.

In this thesis, I will demonstrate that OSM treatment under normoxic conditions induces profound changes in cellular metabolism of PH5CH8 cells. I will show that (1) OSM suppresses glucose and glutamine oxidation via PDH inhibition, (2) demonstrate that OSM enhances reductive glutamine metabolism, (3) HIF-1α is critical for these OSM-induced metabolic changes.

2 Materials and Methods

The following chapter describes the materials and methods for cell culture, metabolite extraction, molecular biology techniques and instrumental analytics.

2.1 Experimental design

The immortalized human PH5CH8 hepatocytes were cultivated under normoxic (21% O_2, 5% CO_2, 37°C) and hypoxic conditions (1% O_2, 5% CO_2, 37°C) in either [U-$^{13}C_6$]glucose, [U-$^{13}C_5$]glutamine labelled medium or unlabelled medium. The metabolites were analysed under four different conditions: in the first two conditions, PH5CH8 cells were transfected with non-targeting siRNA (siCtrl) and stimulated for 36 hours either with 50ng/mL OSM (+OSM) or DPBS (Figure 2.1). In the last two conditions, PH5CH8 were transfected with *HIF-1α* targeting siRNA (siHIF-1α) and stimulated either with 50ng/mL OSM or DPBS for 36 hours. For each condition, PH5CH8 cells were cultivated in triplicates (Figure 2.1).

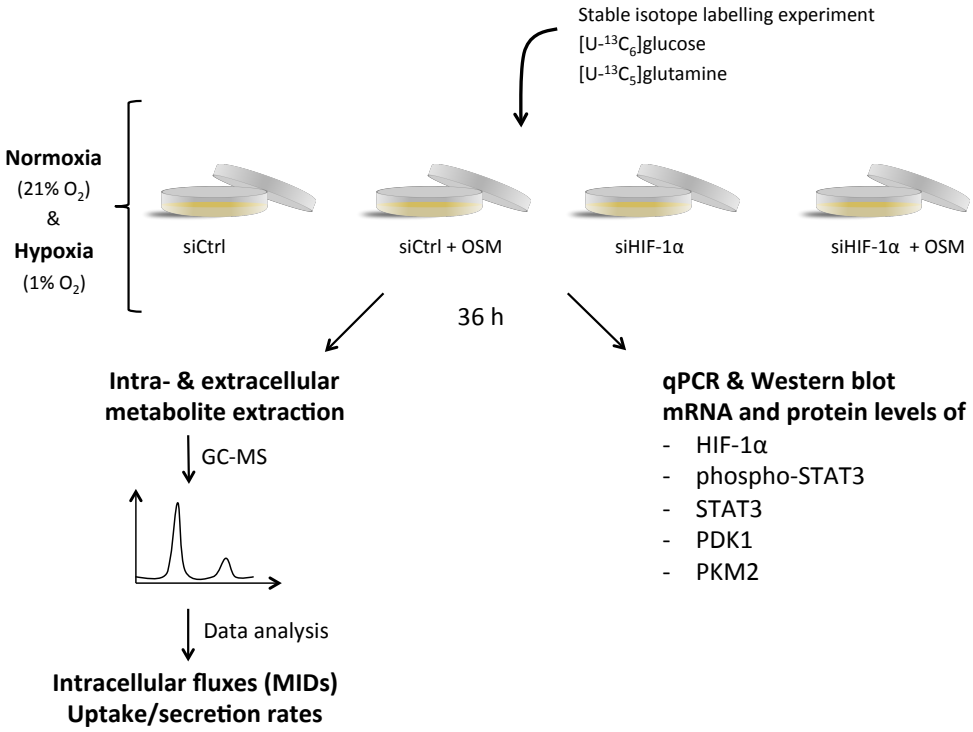

Figure 2.1 Overview of the experimental setup. PH5CH8 were cultured in 12-well plates and transfected with non-targeting siRNA (siCtrl) or siRNA targeting HIF-1α (siHIF-1α). OSM and [U-$^{13}C_6$]glucose, [U-$^{13}C_5$]glutamine or unlabelled media were added to the appropriate plate. The metabolites were extracted after 36 hours and the samples were measured with GC-MS. Expression levels of *HIF-1α*, *PDK1* and *PKM2* were assessed using qPCR and protein levels of HIF-1α, p-STAT3 and STAT3 were assessed using Western blot.

2.2 Cell culture conditions and growth curve

2.2.1 Cell culture conditions

Immortalized human hepatocytes PH5CH8 were maintained in Dulbecco Modified Eagle Medium (Sigma-Aldrich, DMEM 5796; 4.5 g/L glucose, L-glutamine, $NaHCO_3$ and pyridoxine HCl) supplemented with 10% heat-inactivated foetal bovine serum (PAA clone, FBS with low endotoxine). Maintenance of PH5CH8 cells: 1:2 split each second day in T75 flasks (Thermo Scientific). Cells were washed once with 1x Dulbecco's Phosphate Buffered Saline (DPBS) (Invitrogen) and were dispersed with trypsin EDTA (gibco by Life Technologies) for 5 min at 37°C. The cells were grown at 37 °C, 5% CO_2 and humidified atmosphere.

2.2.2 Growth curve

PH5CH8 cells were seeded at a density of $1.9x10^5$ cells/well on a 6-well plate (Delta surface plates, Thermo Scientific) and incubated under normoxic (21% O_2, 5% CO_2, 37°C and humidified atmosphere) conditions. After 6 hours, the cells were treated either with 50 ng/mL OSM or left untreated. The cells were counted at four time points; 0h, 24h, 48h and 72 hours using the cell viability analyzer "Vi-Cell™ XR" (Beckman Coulter).

2.3 *HIF1α* silencing by reverse transfection

For each sample, siRNA-Lipofectamine™ RNAiMAX (Invitrogen) complexes were prepared as follows: 3 µL of Lipofectamine™ RNAiMAX were diluted in 150 µL Opti-MEM I (1x) (Gibco by Life Technologies) and 1 µL siRNA (nontargeting siRNA Santa Cruz Biotechnology, INC.) or 1µL siHIF-1α (20 µM stock concentration, HIF-1α siRNA (h): sc-35561 Santa Cruz Biotechnology, INC.) was diluted in 150 µL Opti-MEM I (final concentration of the nontargeting siRNA and siHIF-1α was 15 nM). Lipofectamine and siRNA were mixed and incubated for 20 minutes at room temperature. 300 µL of Lipofecatmine/siRNA mix were transferred into a 12-well plate and incubated for 5 minutes at room temperature. PH5CH8 cells were then seeded at a density of $7.6x10^4$ cells/well in triplicates directly onto transfection mix and incubated 6 hours at 37 °C, 5% CO_2 and humidified atmosphere. The medium was exchanged to normal culture media and the cells were incubated overnight at 37 °C, 5% CO_2 and humidified atmosphere.

2.4 Preparation of labelling medium and OSM stimulation

For isotopic labelling assisted experiments, PH5CH8 cells were cultured in DMEM 5030 (Sigma-Aldrich, without L-glutamine, glucose, sodium pyruvate and sodium bicarbonate) supplemented with 10% dFBS (dialyzed fetal bovine serum, Invitrogene), 25 mM glucose (Aldrich chemistry) or 25 mM [U-$^{13}C_6$]glucose (Cambridge Isotope Laboratories, INC.) and 4

mM glutamine (Sigma Life Science) or 4 mM [U-$^{13}C_5$]glutamine (Cambridge Isotope Laboratories, INC.), pH 7.4.

Cells were seeded at a density of 7.6x10^4 cells/well and were incubated overnight at 37 °C, 5% CO_2 and humidified atmosphere. Old cell culture medium was removed and cells were washed with DPBS. After adding 975 µL of labelled/unlabelled media to the wells, the cells were stimulated either with 25 µL OSM (PEPROTECH), final concentration 50ng/mL, or with 25 µL DPBS for untreated controls. The cells were stimulated for 36 hours at 37 °C, 5% CO_2 and humidified atmosphere under 21% or 1% O_2 (Hypoxia chamber Jacomex).

2.5 Intracellular and extracellular metabolite extraction

The cell culture medium was removed from the cells, centrifuged for 5 min at maximum speed at 4 °C and the supernatant stored at -80 °C. For intracellular metabolite extraction cells were washed with 1 mL 0.9% NaCl (Sigma Life Science) and quenched with 200 µL ice-cold methanol (Sigma Life Science, Chromasolv, pure grade for HPLC ≥ 99.9%). After adding 200 µL of 4 °C cold water, the cells were detached with a cell scraper (Falcon) and transferred to Eppendorf tubes containing 200 µL ice-cold chloroform (Sigma Life Science, Chromasolv pure grade for HPLC ≥ 99.9%). The extracts were mixed using a Thermomixer (Eppendorf) at 4 °C, 1400 rpm for 20 min and centrifuged at maximum speed for 5 min at 4 °C. 250 µL of the upper polar phase was transferred GC-MS glass vials (Chromatographie Zuberhör Trott CZT) and evaporated under vacuum to dryness at −4 °C using the CentriVap Concentrator (Labconco). The interphase and the non-polar phase were stored at -80°C. Intracellular metabolite extraction of cells incubated at 1% O_2 was performed in the hypoxia chamber.

Extracellular metabolites from medium samples were extracted using ice-cold extraction fluid (8:1 methanol/water) containing the internal standard [U-$^{13}C_5$]ribitol (Omicron Biochemicals, INC.) at a concentration of 10 µg/mL. 20 µL of medium was added to 180 µL ice-cold extraction fluid, vortexed for 10 seconds and centrifuged at maximum speed for 5 min at 4 °C. 50 µL of medium extracts were transferred to GC-MS glass vials and evaporated under vacuum to dryness at −4 °C using the CentriVap Concentrator. In addition an external calibration curve with known glucose and lactate concentration (both starting concentration 27.5 mM, Sigma Life Science) was prepared in serial dilution of five 1:2 dilutions in H_2O and extracted using the extraction fluid (8:1 methanol/water + [U-$^{13}C_5$]ribitol).

2.6 Metabolite derivatization

Derivatization was carried out as previously described (André Wegner *et al.*, 2014) (38). Briefly, the derivatization of intra- and extracellular metabolites was performed using a multipurpose sampler (Gerstel). The dried intracellular metabolite extracts were derivatized with N-tert- MTBSTFA. For TBDMS derivatization, dried extracts were dissolved in 15 µl pyridine, containing 20 mg/ml methoxyamine hydrochloride (MOX), at 55 °C for 60 min under shaking. After additional 15 µl MTBSTFA with 1% tert-Butyldimethylchlorosilane samples were incubated at 55 °C for 60 min under continuous shaking. The dried extracellular metabolite extracts were derivatized with MSTFA. For TMS derivatization, the extracts were dissolved in 15 µl pyridine, containing 20 mg/ml MOX and incubated for 60 min at 40 °C under shaking. Then, 15 µl MSTFA was added and the samples were incubated at 40 °C for 30 min under continuous shaking. The chemicals for metabolite derivatisation were all obtained from Sigma-Aldrich.

2.7 Gas chromatography-mass spectrometry (GC-MS) analysis

GC-MS measurement was carried out as previously described (André Wegner *et al.*, 2014) (38). For each condition, three replicates were measured by GC-MS using the Agilent 7890A GC system connected to Agilent 5975C inert XL MSD quadrupole mass spectrometer under electron impact (EI) ionization. 1 µL of the samples were injected into a Split/Splitless inlet operating in split mode (split ratio 3:1; MOX/TMS derivatization) or splitless mode (MOX/TBDMS derivatization) at 270 °C. Helium was used as carrier gas with a constant flow rate of 1 ml/min. The GC was equipped with a 30 m x 0.25 mm I.D. x 0.25 µm film thickness DB-35MS capillary column + 5 m DuraGuard capillary in front of the analytical column.

For MOX/TBDMS derivatized intracellular samples, the GC oven temperature was held at 100 °C for 3 min and increased to 300 °C at 3.5 °C/min.

For MOX/TMS derivatized extracellular samples, the temperature was held at 80 °C for 6 min and increased to 300 °C at 6 °C/min.

After 10 min, the temperature was increased at 10 °C/min followed by an additional constant temperature period at 325 °C for 4 min. The mass selective detector (MSD) was operating under electron ionization at 70 eV. The MS source was held at 230 °C and the quadrupole at 150 °C. Full scan mass spectra were acquired from m/z 70 to 800. The total run time for MOX/TMS derivatized samples was 59.167 min and 60.143 min for MOX/TBDMS derivatized samples. The mass detector operated in single ion monitoring mode (SIM).

2.8 Mass isotopomer distribution analysis

The data was processed using the MetaboliteDetector software package (Hiller *et al*., 2009) (39). The detected peaks were identified by comparing the chromatogram and the retention time to the reference compound library. The compound detection was performed with the following deconvolution settings: peak thresholds 5, minimal peak height 5, bins 10, deconvolution width 5. All intracellular metabolites were identified as TBDMS derivatives (Table 2.1). Mass isotopomer distributions were determined and corrected for natural isotope abundance using MetaboliteDetector.

Weighted carbon contribution corresponds to $\frac{1}{n}\sum_{i=0}^{n} \mathrm{M_i}$ * i, where i is the number of stable isotopes in the isotopologue and M its relative isotopologue abundance using [U-$^{13}C_6$]glucose or [U-$^{13}C_5$]glutamine tracer.

Table 2.1 GC-MS metabolites and fragments used for isotope quantification.

Compound	Fragment (m/z)	Formula
Alanine 2TBDMS	260 - 268	$C_{11}H_{26}NO_2Si_2$
	232 - 239	$C_{10}H_{26}NOSi_2$
Aspartic acid 3TBDMS	418 - 428	$C_{18}H_{40}NO_4Si_3$
	302 - 310	$C_{14}H_{32}NO_2Si_2$
Citric acid 4TBDMS	591 - 602	$C_{26}H_{54}O_7Si_4$
Fumaric acid 2TBDMS	287 - 297	$C_{12}H_{23}O_4Si_2$
Glutamine 3TBDMS	431 - 441	$C_{19}H_{43}N_2O_3Si_3$
Glutamic acid 3TBDMS	432 - 442	$C_{19}H_{42}NO_4Si_3$
	330 - 340	$C_{16}H_{36}NO_2Si_2$
Malic acid 3TBDMS	419 - 428	$C_{18}H_{39}O_5Si_3$
Lactic acid 2TBDMS	261 - 269	$C_{11}H_{25}O_3Si_2$

All extracellular metabolites were identified as TMS derivatives (Table 2.2).

Table 2.2 GC-MS extracellular metabolites, fragments and formula.

Compound	Fragments (m/z)
Lactic acid 2TMS	117.1 191.1 219.1
Valine 2TMS	218.1 144.1 246.1
Leucine 2TMS	158.1 218.1 260.1
Isoleucine 2TMS	158.1 218.1 260.1
[U$^{13}C_5$]Ribitol 5TMS	207.1 220.1 323.2
Glucose 1MeOX 5TMS	205.1 217.1 319.2

2.9 Quantitative real-time PCR

The interphases were washed with 300 µL methanol, centrifuged at maximum speed at 4°C for 5 min and the pellets were dried under the chemical hood. Total RNA was extracted from the interphases using the RNA Purification kit RNeasy^{R} Minikit (QIAGEN) following manufacture's instruction. RNA concentration was measured using the NanoDrop (Thermo Scientific). cDNA was prepared using 1 µL of oligonucleotide (oligo DT 50 µM, Invitrogen), 600 ng total RNA and 1 µL dNTP (deoxyribonucleotide triphosphate 10mM, Sigma Life Science) mix and RNase free water (Sigma Life Science) up to 13 µL. The samples were denatured at 65 °C for 5 minutes and incubated on ice for 1 minute. Reverse transcription was performed using 4 µL 5x First-Strand buffer (250 mM Tris-HCl (pH 8.3 at room temperature), 375 mM KCl, 15 mM $MgCl_2$), 1 µL 0.1 M DTT (Invitrogen), 1 µL RNaseOUT^{TM} Recombinant RNase Inhibitor (Invitrogen) and 1 µL SuperScript^{TM} III RT (Invitrogen) for 60 minutes at 50°C and inactivated at 70°C for 15 minutes. The cDNA concentration was measured using NanoDrop. cDNA (amount of cDNA used for qPCR: 600 ng) was used as a template for quantitative real-time PCR analysis under the conditions in Table 2.4 using the LightCycler 480 detection system. The primer pairs were used for quantitative real-time PCR as listed in Table 2.3. For each primer, a master mix was prepared as follows: For each sample 0.5 µL of forward primer, 0.5 µL of reverse primer, 7 µL ddH_2O and 10µL Syber Green (BIO-RAD). 2 µL of cDNA were used per PCR reaction.

Table 2.3 Primer sequences for qPCR.

Gene Symbol	Sequence (5'-3')	Supplier
Human HIF1α	forward CGTTCCTTCGATCAGTTGTC reverse TCAGTGGTGGCAGTGGTAGT	Eurogentec
Human PDK1	forward GCACTCTTTATTGTTTGGTGG reverse ACGCCTAGCATTTTCATAGC	Eurogentec
Human PKM2	forward CAGAGGCTGCCATCTACCAC reverse CCAGACTTGGTGAGGACGAT	Eurogentec
Human PKM1	forward GAGGCAGCCATGTTCCAC reverse TGCCAGACTCCGTCAGAACT	Eurogentec
Human L27 (housekeeping gene)	forward CTG GTG GCT GGA ATT GAC reverse ACA GAG TAC CTT GTG GGC	Eurogentec

Table 2.4 qPCR conditions.

temperature	time	cycles
95°C	5 min	
95°C	30 s	
60°C	30 s	45
72°C	30 s	
95°C	15 s	
40°C	1h 30 min	

2.10 Western Blot

2.10.1 Protein extraction

PH5CH8 cells were seeded at a density of $1.9x10^5$ cells/well on a 6-well plate, transfected with non-targeting or HIF-1α targeting siRNA and stimulated with OSM for 36 hours under normoxia and hypoxia (1% O_2). Proteins were extracted with 120 µL of mammalian protein extraction reagent (M-PER) (Thermo Scientific) supplemented with proteinase inhibitors (Roche) and extracts were mixed 10 min, 1.400 rpm at 4 °C using the Thermomixer. After centrifuging for 10 min at maximum speed and at 4 °C, the supernatant was transferred into an Eppendorf tube and used for SDS-PAGE. The protein concentration was measured with the Nanodrop.

A positive control for HIF-1α was included. HeLa cells were stimulated with 75 µM cobalt chloride (Sigma Life Science), incubate at 37 °C, 5% CO_2 and humidified atmosphere for 4 hours. Proteins were extracted as described above.

2.10.2 SDS-Page

Proteins were separated by sodium dodecyl sulfate polyacrylamide gel electrophoresis (SDS-Page). Protein extracts were diluted in 5x Laemmli buffer (Trizma HCl, ß-mercaptoethanol, glycerol, SDS, Bromophenol red, ddH_2O) to load 20 µg of protein and denatured for 5 min at 95 °C. 15 µL of protein extract were loaded on a 10% Mini-Protean TGX Precast Gel (BIO-RAD). Precision Plus protein kaleidoscope standards (BIO-RAD) severed as marker. The gel ran 15 minutes at 90 V and 60 min at 120 V.

2.10.3 Western Blotting

Separated proteins were transferred to a PVDF membrane (Immobilon PVDF membranes), which was activated for 30 seconds in 100% MeOH (Sigma-Aldrich). The transfer was performed at 80V in 1x transfer buffer with 20% MeOH (10x transfer buffer: 200mM Trizma-Base, 1.92mM Glycine, ddH_2O to 1 L, from Sigma Life Science). The blot ran at 80 V for one hour. The PVDF membrane was blocked with 10% BSA (Albumin Fraction V (pH 7.0) blotting grade, from AplliChem Panreac) in 1x TBS-T with 0.1% Tween (10x TBS: 200mM Trizma-

Base, 137 M NaCl, ddH2O to 1 L) for 1 hour at room temperature, washed three times with 1x TBST and incubated with primary antibodies against HIF-1α (BD Bioscience, purified Mouse Anti-human HIF-1α) diluted 1:1000 in 5% BSA in TBS-T, phospho-STAT3 (cell signaling, purified rabbit anti-human) diluted 1:1000 in 5% BSA in TBS-T and ß-actin (Sigma, purified mouse anti-human) diluted 1:5000 in 5% milk in TBS-T. The blots were incubated over night at 4°C with constant shaking. The membranes were washed with 1x TBS-T and incubated with the secondary antibodies anti-mouse coupled to horseradish peroxidase (HRP) diluted 1:5000 in 5% BSA or 5% milk, depending on the first antibody, and anti-rabbit coupled to HRP diluted 1:5000 in 5% BSA for 1 hour at room temperature. After three washing steps with 1x TBS-T, the secondary antibodies were detected using Luminol ECL reagent (ECL™ Western blotting Detection Reagent, GE healthcare) with Odyssey 2800 (Licor), channel 700 for 30 seconds and Chemi for 2 minutes.

The quantification of the protein bands from the membrane was performed using ImageJ (Image Processing and Analysis in Java, http://imagej.nih.gov/ij) software, providing the band intensities. The level of HIF- 1α, STAT3 and p-STAT3 proteins were normalized to ß-actin protein level. Then p-STAT3 protein level was normalized to the STAT3 protein level.

3 Results

The aim of this master's thesis was to investigate the role of HIF-1α in OSM-induced metabolic reprogramming of human hepatocytes.

Since HIF-1α is the master regulator of the cellular response to low oxygen levels, I hypothesized that OSM reprograms cellular metabolism of the immortalized human hepatocyte PH5CH8 cell line to a hypoxia-like metabolic phenotype and that those changes are mediated by HIF-1α.

3.1 OSM treatment increases transcription and protein levels of HIF-1α

Based on the previous finding that *HIF-1α* mRNA and protein levels are increased in response to OSM-mediated STAT3 signalling under normoxic conditions (Vollmer, Kappler *et al*., 2009)(8) in immortalized hepatocytes and hepatocellular carcinoma cells (HepG2), I first aimed to validate whether OSM increases the expression level of *HIF-1α* in PH5CH8 cells. The relative expression level of *HIF-1α* was significantly (Welch's t-test; p = 0.024) increased upon OSM stimulation at 21% O_2 (Figure 3.1). At 1% O_2, *HIF-1α* transcription was also induced by OSM (Welch's t-test; p = 0.005). However, at 1% O_2 the overall *HIF-1α* mRNA level was decreased as compared to 21% O_2 (Figure 3.1).

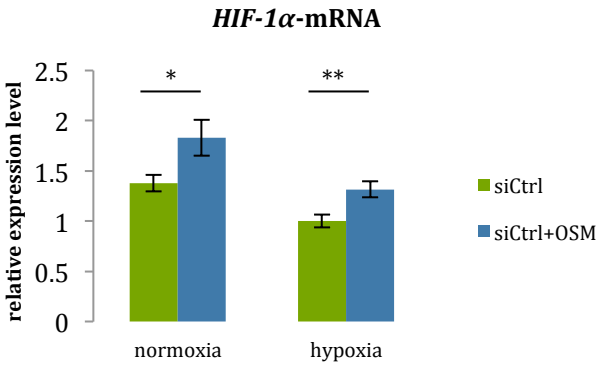

Figure 3.1 OSM induces *HIF-1α* up-regulation in human hepatocytes PH5CH8 under normoxic and hypoxic conditions. PH5CH8 cells were treated either with OSM (siCtrl+OSM) or DPBS (siCtrl) in normoxia and hypoxia. The fold change was calculated relative to the untreated control. Error bars represent the standard deviation from at least two independent replicates (n≥2), Welch's t-test; *p < 0.05, **p < 0.01.

Subsequently, I investigated whether OSM induces STAT3 phosphorylation and increases HIF-1α protein levels under normoxic conditions. OSM significantly induced STAT3 phosphorylation under both normoxia (Welch's t-test; p = 3E-05) and hypoxia (Welch's t-test; p = 2E-04) (Figure 3.2A and C), whereas HIF-1α protein levels were solely increased by OSM under normoxia (Welch's t-test; p = 0.008) (Figure 3.2A, B and C).

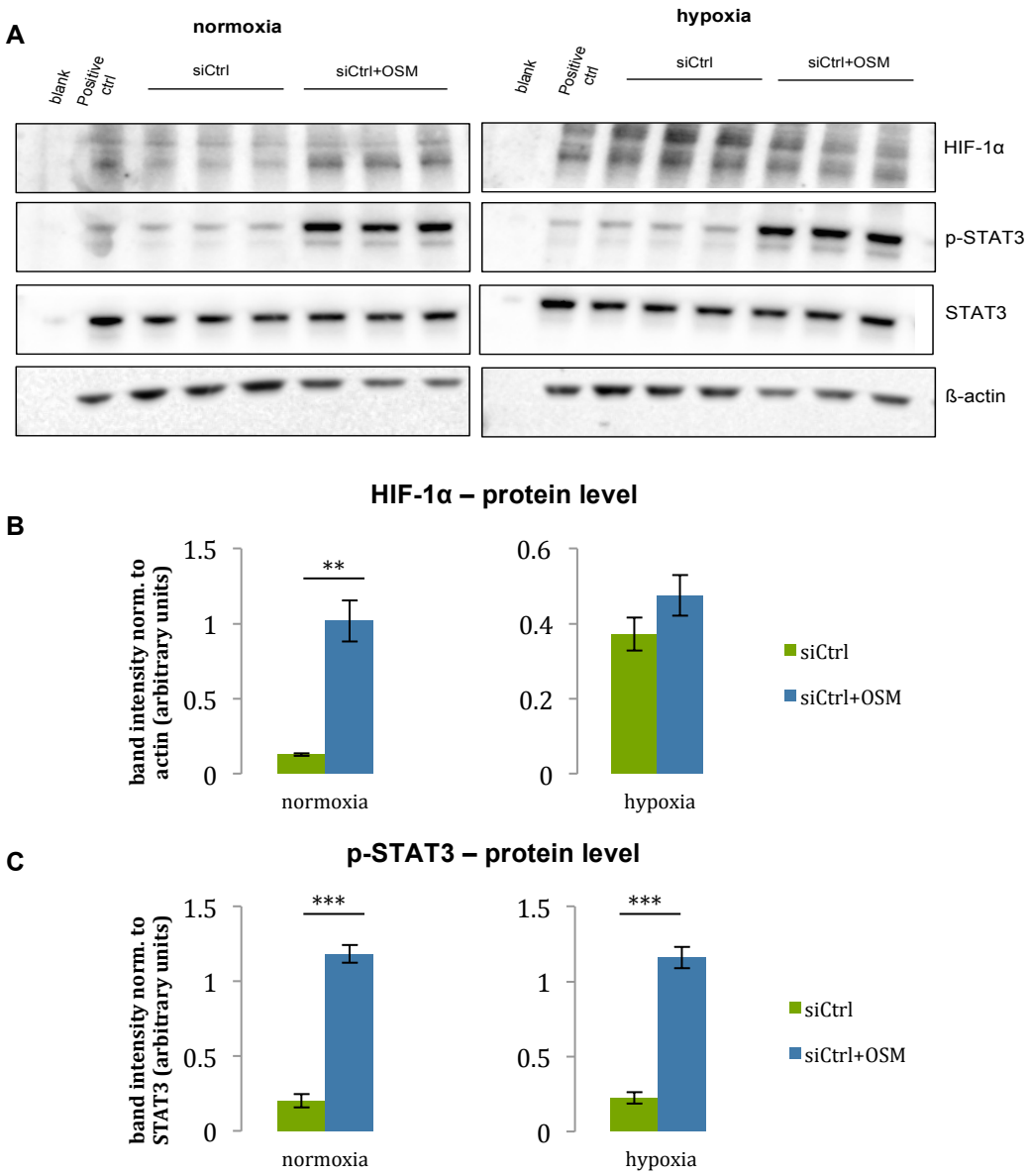

Figure 3.2 OSM stimulation results in an increase of HIF-1α protein levels under normoxia. (A) Western blot for HIF-1α, STAT3 and p-STAT3. PH5CH8 cells were treated either with OSM (siCtrl+OSM) or with DPBS (siCtrl) in normoxia or hypoxia. As positive control HeLa cells were treated with $CoCl_2$. (B)&(C) Quantification of HIF-1α and phospho-STAT3 protein levels in PH5CH8 cells. HIF-1α levels were normalized to ß-actin and p-STAT3 was normalized to STAT3. Error bars represent the standard deviation of at least two biological replicates), Welch's t-test; *p < 0.05, **p < 0.01 and ***p < 0.001.

3.2 OSM supresses glucose oxidation via PDH inhibition

Since HIF-1α is known to suppress glucose oxidation in the TCA cycle (10), I first studied the effect of OSM treatment on glucose oxidation in PH5CH8 cells using stable isotope assisted metabolomics. Therefore, I cultured PH5CH8 cells in medium supplemented with 25 mM [U-$^{13}C_6$]glucose and stimulated either with OSM (siCtrl+OSM) or with DPBS (siCtrl) (Figure 2.1). After GC-MS measurements, I quantified the isotopic enrichment in form of MIDs for several TCA cycle metabolites, including citrate, α-ketoglutarate, malate, fumarate, aspartate, glutamate and glutamine.

At 21% O_2, I observed significantly (Welch's t-test; p = 0.004) increased M0 citrate isotopologues in OSM-treated cells compared to the control (Figure 3.3A). Increased M0 citrate isotopologues propagated to the analysed downstream metabolites of the TCA cycle α-ketoglutarate, fumarate, malate, glutamate and aspartate (Figure 3.4 and Supplemental Table 1.). M0 isotopologues represent the fraction of citrate not enriched from [U-$^{13}C_6$]glucose, suggesting that upon OSM stimulation the majority of citrate is metabolized from an alternative carbon source. To further analyse the glucose carbon contribution to citrate, I quantified the weighted contribution of glucose-derived carbons to citrate (2.8 mass isotopomer distribution analysis). In line with the increased M0 isotopologues of citrate, I observed significantly (Welch's t-test; p = 0.006) decreased glucose-derived carbon in citrate in response to OSM treatment (Figure 3.5).

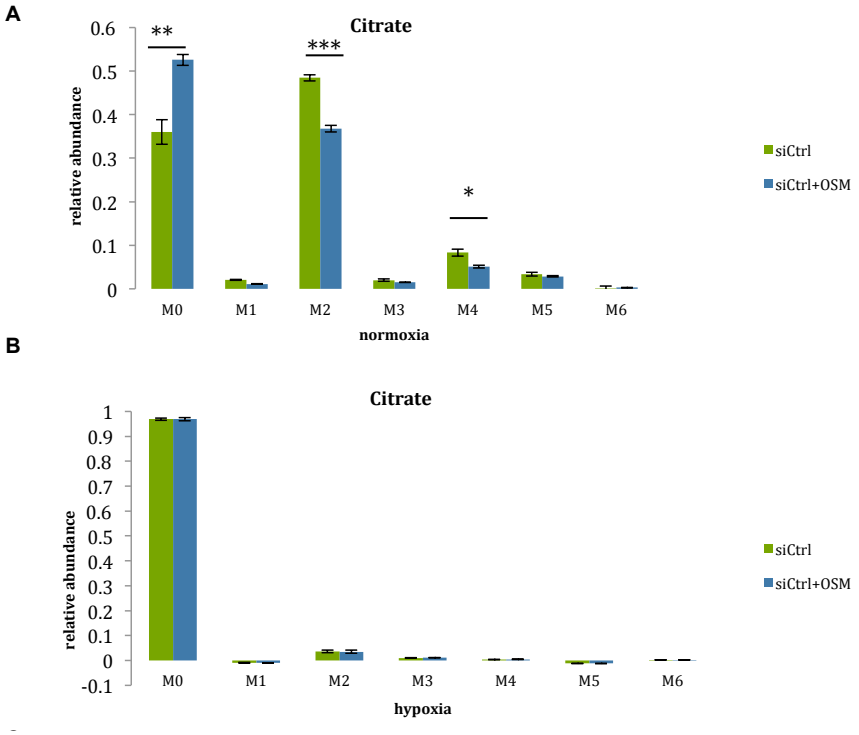

Figure 3.3 Mass isotopomer distributions of citrate from [U-$^{13}C_6$]glucose in (A) normoxia and (B) hypoxia. Error bars represent the standard deviation from at least two independent replicates (n≥2). Welch's t-test, *p < 0.05, **p < 0.01, ***p < 0.001

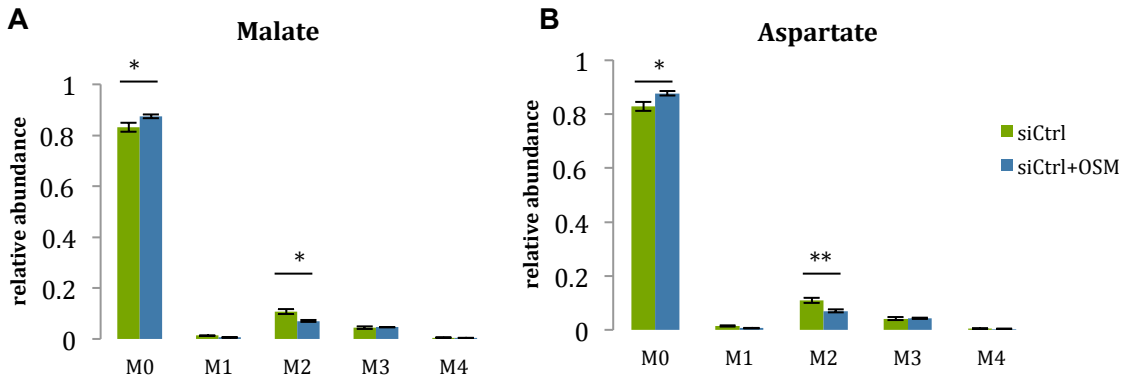

Figure 3.4 Mass isotopomer distribution of (A) malate and (B) aspartate in normoxia from [U-$^{13}C_6$]glucose. Error bars represent the standard deviation from at least two independent replicates (n≥2). Welch's t-test, *p < 0.05, **p < 0.01.

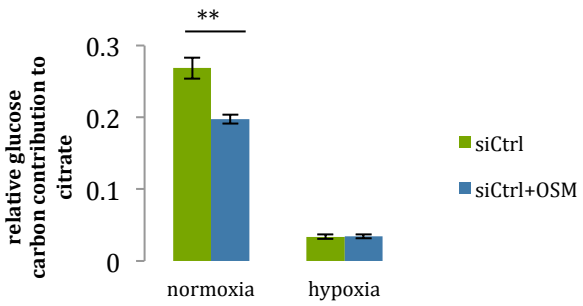

Figure 3.5 Effect of OSM stimulation on relative glucose carbon contribution to citrate under normoxia and hypoxia. Weighted carbon contribution was calculated as described in section 2.8. Error bars represent the standard deviation from at least two independent replicates (n≥2), Welch's t-test; *p < 0.05, **p < 0.01.

Glucose-derived carbons can enter the TCA cycle via two ways: either through pyruvate dehydrogenase (PDH) complex or through pyruvate carboxylase (PC). In order to distinguish both pathways and investigate whether the observed reduced glucose carbon contribution to citrate results from reduced PC or reduced PDH activity, I analysed the labelling pattern of citrate (Figure 3.6A). If PC is active, [$^{13}C_3$]pyruvate is carboxylated to [$^{13}C_3$]oxaloacetate and ,thus , condensation of [$^{13}C_3$]oxaloacetate and unlabelled acetyl-CoA results in M3 citrate. In contrast, M2 citrate isotopologues result from [U-$^{13}C_6$]glucose-derived [$^{13}C_3$]pyruvate that is metabolized to [$^{13}C_2$]acetyl-CoA. Subsequently, [$^{13}C_2$]acetyl-CoA is condensed with unlabelled oxaloacetate to [$^{13}C_2$]citrate (M2 isotopologues). M4 citrate is metabolized in a

second round of the TCA cycle, resulting from [$^{13}C_2$]acetyl-CoA and [$^{13}C_2$]oxaloacetate via citrate synthase. In addition, M5 isotopologues of citrate result from [$^{13}C_3$]oxaloacetate and [$^{13}C_3$]pyruvate-derived [$^{13}C_2$]acetyl-CoA, thereby giving a readout of the combined activity of PDH and PC (Figure 3.6A). I observed that OSM stimulation resulted in reduced M2 and M4 isotopologues of citrate compared to the control (A). At 21% O_2, I did not observe any difference in M3 and M5 citrate isotopologues upon OSM stimulation (A), suggesting that the reduced glucose carbon contribution to citrate is caused by decreased PDH activity. To avoid that the observed differences are effects from the overall enrichment, I normalized the M2 and M3 citrate isotopologues to M3 lactate isotopologues and observed significantly (Welch's t-test; p = 5E-05) reduced PDH activity (Figure 3.6D), but no effect on PC activity (Figure 3.6B) in OSM-stimulated cells under normoxic conditions compared to the control. The overall PC activity was relatively low under normoxic conditions (Figure 3.6B) suggesting that pyruvate-derived carbon almost exclusively enters the TCA cycle through acetyl-CoA and not through oxaloacetate.

In response to OSM stimulation, reduced amount of M2 isotopologues propagated to downstream metabolites in the TCA cycle, including α-ketoglutarate, fumarate, malate, glutamate and aspartate (Figure 3.4 and Supplemental table 2.). These data suggest that reduced PDH activity is responsible for the observed reduced glucose carbon contribution to citrate.

Since the PDH complex is mainly regulated post-translationally by PDK1, which phosphorylates the PDH E1α subunit, thereby inactivating the PDH enzyme complex(16), I next determined the expression level of *PDK1* (Figure 3.6C). In line with decreased M2 isotopologues of citrate, I observed significantly (Welch's t-test; p = 0.0204) increased *PDK1* transcription in response to OSM stimulation under normoxia (Figure 3.6C).

Altogether, this data strongly suggests that OSM treatment increases the expression of *PDK1* under normoxia, thereby inhibiting PDH and limiting glucose oxidation in the TCA cycle.

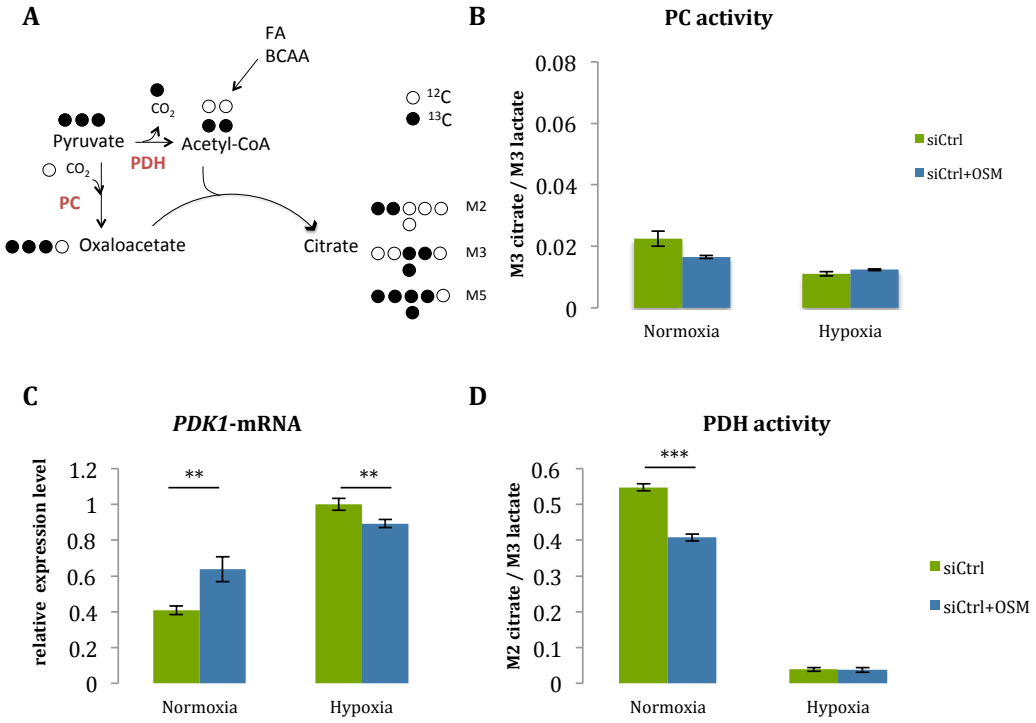

Figure 3.6 Effect of OSM stimulation on PC and PDH activity, and *PDK1* transcription in normoxic and hypoxic conditions. (A) Carbon atom transitions of PC and PDH. (B) Relative PC activity, determined by the ratio of M3 isotopologues of citrate to M3 isotopologues of lactate, from [U-$^{13}C_6$]glucose. (C) qPCR of *PDK1* mRNA. (D) PDH activity determined by the ratio of M2 isotopologues of citrate to M3 isotopologues of lactate, from [U-$^{13}C_6$]glucose. Error bars represent the standard deviation from at least two independent replicates (n≥2), Welch's t-test; **p < 0.01 and ***p < 0.001.

In order to investigate whether the OSM-induced suppression of glucose oxidation is comparable to the metabolic phenotype induced by hypoxia, I analysed the MIDs of citrate and downstream metabolites at 1% O_2. Under hypoxia, the majority of citrate was not enriched from [U-$^{13}C_6$]glucose, suggesting that most of the citrate carbon is not derived from glucose (Figure 3.3B). In agreement with the high amount of M0 isotopologues of citrate, I observed increased *PDK1* transcription in PH5CH8 cells grown under hypoxia (Figure 3.5 and 3.6B). Consequently, PDH activity was suppressed and glucose oxidation limited (Figure 3.6D). As a result of reduced PDH activity, M2 and M4 isotopologues of citrate and downstream metabolites of the TCA cycle were highly decreased at 1% O_2 compared to 21% O_2 (Figure 3.3B and Supplemental Table 3.). At 1% O_2, I did not observe any effect on glucose oxidation and PDH activity upon OSM treatment. However, I observed a slight

decrease in *PDK1* transcription in OSM-stimulated cells under hypoxia compared to the control (Figure 3.6C).

OSM-induced PDK1 up-regulation and PDH inhibition represented an intermediate state between cells grown under normoxia and hypoxia. The resulting changes in MID of citrate, including increased M0 and decreased M2 or M4 isotopologues, and the reduced glucose oxidation induced by OSM under normoxia were less pronounced compared to the changes induced by hypoxia.

Collectively, these data show that the level of glucose oxidation and PDH activity upon OSM treatment under normoxia represents an intermediate metabolic phenotype between normoxia and hypoxia.

3.3 Glutamine oxidation in the TCA cycle is reduced in response to OSM stimulation

Since OSM stimulation suppresses glucose oxidation in the TCA cycle by PDH inhibition, I next studied whether this effect was compensated by an increased glutamine oxidation. Therefore, PH5CH8 cells were cultured in medium containing 4 mM [U-$^{13}C_5$]glutamine under normoxic and hypoxic conditions (Figure 2.1). OSM-treated cells exhibited significantly reduced M4 and M2 citrate isotopologues compared to the control under normoxia (Welch's t-test; M2 p = 0.002 / M4 p = 3E-05) (Figure 3.7A). [$^{13}C_4$]citrate results from [U-$^{13}C_5$]glutamine-derived [$^{13}C_5$]α-ketoglutarate that is eventually converted in the TCA cycle to [$^{13}C_4$]oxaloacetate. Subsequently, [$^{13}C_4$]oxaloacetate and unlabelled acetyl-CoA are condensed to [$^{13}C_4$]citrate (Figure3.8B), thereby providing a readout of relative glutamine oxidation in the TCA cycle. Furthermore, I observed that under normoxia reduced M2 and M4 isotopologues propagated to the downstream metabolites fumarate, malate, and aspartate upon OSM stimulation (Supplemental Table 2.).

To exclude bias from the overall enrichment, I normalized the M4 isotopologues of citrate with the M5 isotopologues of α-ketoglutarate. I observed a significant (Welch's t-test; p = 5E-07) drop in the M4 citrate to M5 α-ketoglutarate ratio (Figure 3.8A), suggesting a decrease in relative glutamine oxidation.

At 1% O_2, I observed a significant (Welch's t-test; p = 1E-06) drop of the M4 citrate to M5 α-ketoglutarate ratio compared to 21% O_2 (Figure3.7B), pointing to suppressed glutamine oxidation in hypoxic conditions. There was no difference in glutamine oxidation under hypoxia upon OSM treatment (Figure 3.8A).

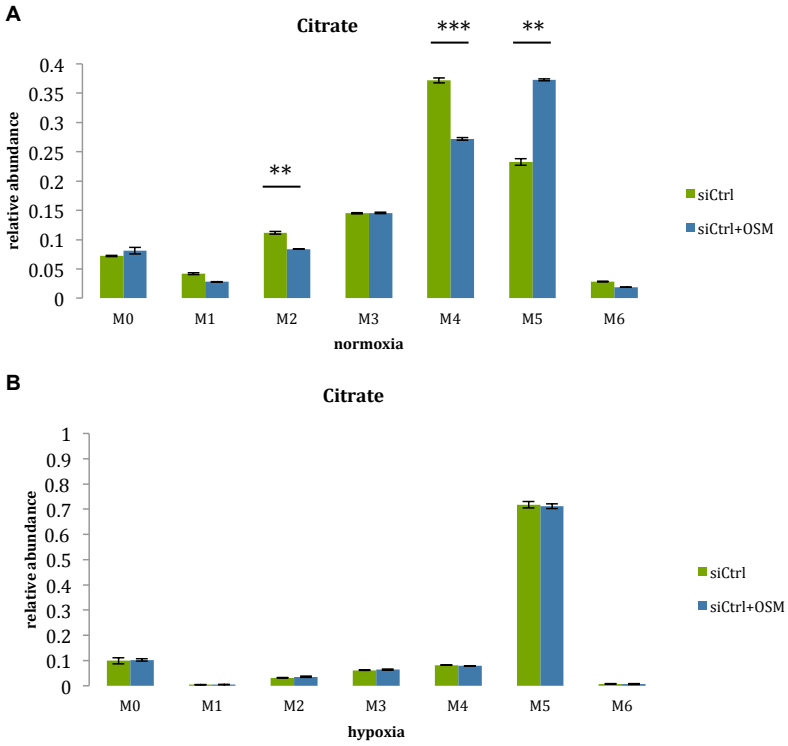

Figure 3.7 Mass isotopomer distributions of citrate from [U-$^{13}C_5$]glutamine in (A) normoxic and (B) hypoxic conditions. Error bars represent the standard deviation from at least two independent replicates (n≥2). Welch's t-test; **p < 0.01, ***p < 0.001

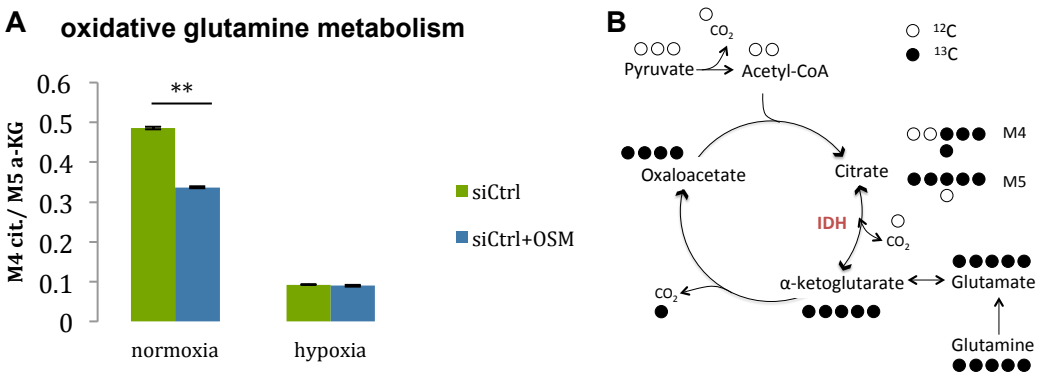

Figure 3.8 Effect of OSM on oxidative glutamine metabolism under normoxia and hypoxia. (A) Relative glutamine oxidation in the TCA cycle, determined by the ratio of M4 isotopologues of citrate to M5 isotopologues of α-ketoglutarate from [U-$^{13}C_5$]glutamine. Error bars represent the standard deviation from at least two independent replicates (n≥2), Welch's t-test; *p < 0.05, **p < 0.01. (B) Simplified scheme of TCA cycle with carbon atom transitions of oxidative and reductive glutamine metabolism.

3.4 OSM stimulation increases reductive glutamine metabolism

Although glutamine oxidation was significantly (Welch's t-test; p = 5E-07) decreased, the fractional contribution of glutamine-derived carbon to citrate was moderately increased in the OSM-treated cells compared to the control (Welch's t-Test; p = 0.001) (Figure 3.9). These results indicate that in OSM-stimulated cells, citrate is derived from glutamine through an alternative pathway, other than the oxidative TCA cycle. Therefore, I investigated whether OSM stimulation would lead to increased reductive glutamine metabolism under normoxia. Citrate can be metabolized through reductive carboxylation of α-ketoglutarate via IDH (Figure 3.7C), which leads to M5 isotopologues of citrate. Glutamine-derived [$^{13}C_5$]α-ketoglutarate and unlabelled CO_2 are metabolized to [$^{13}C_5$]isocitrate via IDH, followed by isomerization of [$^{13}C_5$]isocitrate to [$^{13}C_5$]citrate by aconitase (Figure 3.7C). I observed that the ratio of M5 citrate to M5 α-ketoglutarate was significantly (Welch's t-test; p = 2E-04) increased upon OSM stimulation as compared to the untreated control (Figure 3.10).

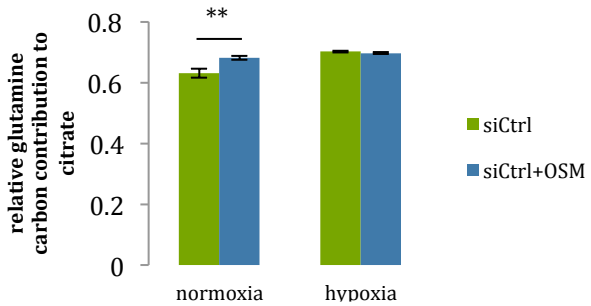

Figure 3.9 Effect of OSM on relative glutamine carbon contribution to citrate under normoxia and hypoxia. Error bars represent the standard deviation from at least two independent replicates (n≥2), Welch's t-test; *p < 0.05, **p < 0.01.

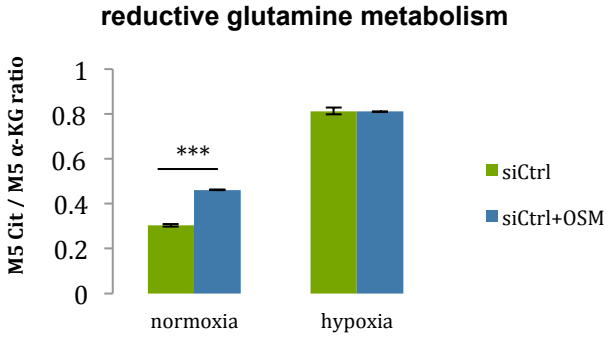

Figure 3.10 Effect of OSM stimulation on reductive glutamine metabolism. Relative reductive flux, determined by the ratio of M5 isotopologues of citrate to M5 isotopologue of α-ketoglutarate in normoxia and hypoxia from [U-$^{13}C_5$]glutamine. Error bars represent the standard deviation from at least two independent replicates (n≥2), Welch's t-test; *p < 0.05, **p < 0.01 and ***p < 0.001.

In line with these results, M3 isotopologues of fumarate, malate and aspartate were also significantly increased upon OSM stimulation under normoxia (Welch's t-test; malate p = 6E-05 / aspartate p = 3E-04) (Figure 3.11 an Supplemental Table 2.). M3 isotopologues of fumarate, malate, and aspartate derive from [$^{13}C_5$]citrate, which is cleaved to [$^{13}C_3$]oxaloacetate and [$^{13}C_2$]acetyl-CoA by citrate lyase.

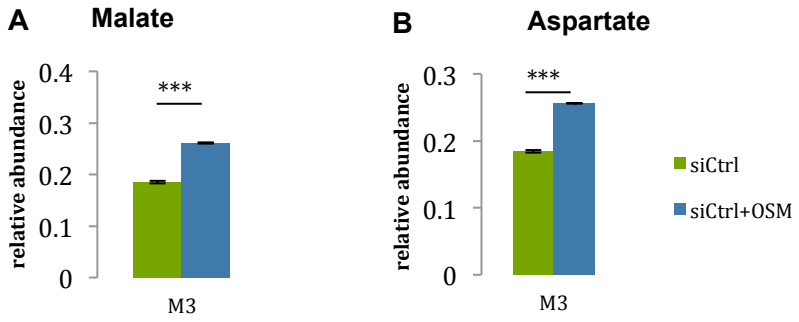

Figure 3.11 Effect of OSM on M3 isotopologue abundances of (A) malate and (B) aspartate in normoxic conditions from [U-$^{13}C_5$]glutamine. Error bars represent the standard deviation from at least two independent replicates (n≥2), Welch's t-test; *p < 0.05, **p < 0.01 and ***p < 0.001.

These results strongly suggest that under normoxia reduced glucose and glutamine oxidation via PDH inhibition is at least partly compensated by an increased reductive IDH flux to maintain the citrate pool upon OSM stimulation.

Under hypoxic conditions, the M5 citrate to M5 α-ketoglutarate ratio was significantly (Welch's t-test; p = 0.0005) increased compared to OSM-stimulated cells under normoxia (Figure 3.10). I did not observe any effects of OSM treatment on reductive glutamine metabolism under hypoxia (Figure 3.10).

3.5 OSM increases glucose uptake and lactate secretion

To analyse whether OSM stimulation enhances glucose uptake and lactate production, I measured glucose consumption and lactate secretion in PH5CH8 cells. Glucose uptake was slightly increased by OSM treatment (Figure 3.12A). In line with increased glucose uptake and reduced glucose oxidation in the TCA cycle, I observed slightly increased lactate secretion upon OSM stimulation under normoxic conditions (Figure 3.12B). These results indicate that PH5CH8 cells exhibit a more glycolytic phenotype in response to OSM stimulation.

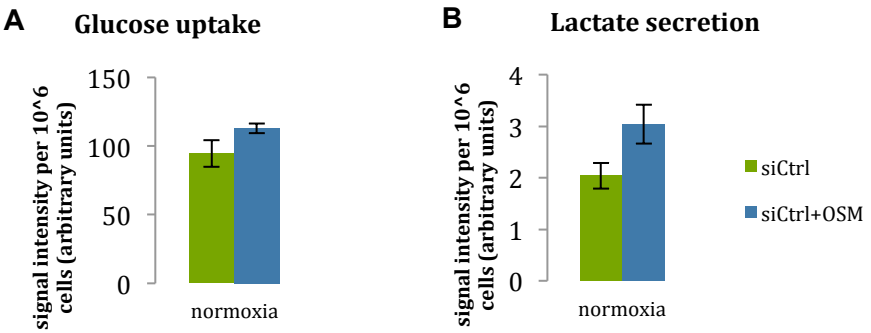

Figure 3.12 Effect of OSM stimulation on glucose uptake and lactate secretion under normoxia. (A) Glucose uptake and (B) lactate secretion determined by GC-MS. Signal intensities were normalized to cell numbers. Error bars represent the standard deviation from at least two independent replicates (n≥2).

Since the expression of *PKM2* is increased in many human cancer cells and is associated with increased glucose uptake and increased lactate production (23), I investigated whether OSM stimulation leads to increased *PKM2* transcription in PH5CH8 cells. Therefore, I determined the mRNA levels of *PKM2* in normoxic and hypoxic conditions by qPCR. I did not observe any difference in the expression of *PKM2* between OSM-stimulated and untreated cells under normoxia. However under hypoxia, *PKM2* mRNA levels were increased as compared to the cells cultured in normoxia, but remained unaffected upon OSM stimulation (Figure 3.13).

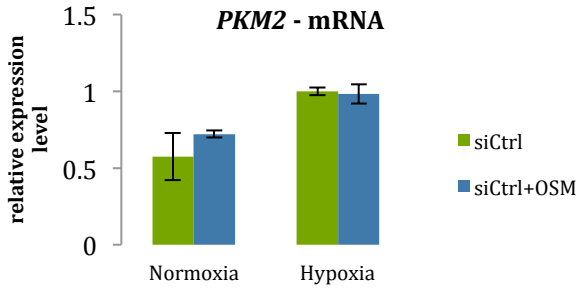

Figure 3.13 OSM stimulation on relative *PKM2* mRNA expression levels under hypoxia and normoxia.

3.6 OSM stimulation does not increase the proliferation rate of PH5CH8

Since IL-6 stimulation was shown to increase hepatocyte proliferation (40), I examined whether OSM stimulation contributes to increased proliferation rates of PH5CH8 cells. Therefor, I cultured PH5CH8 cells either with OSM or with DPBS and counted cells 24 and

48 hours after OSM stimulation. I observed no significant effect on cell proliferation upon OSM stimulation under normoxia (Figure 3.14).

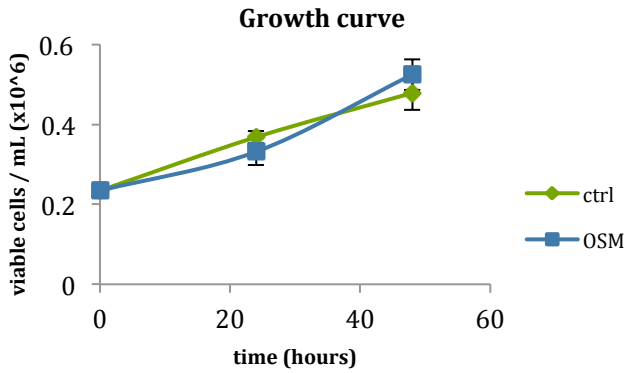

Figure 3.14 Effect of OSM treatment on PH5CH8 growth under normoxia. PH5CH8 cells were treated either with OSM or with DPBS. The cells were counted at three time points; 0, 24 and 48 hours. Error bars represent the standard deviation from three independent replicates.

3.7 HIF-1α is critical for the OSM-induced metabolic changes

To prove the importance of HIF-1 α for the OSM-induced metabolic reprogramming in immortalized human hepatocytes, I performed silencing experiments using non-targeting and *HIF-1α* targeting siRNA. Silencing of *HIF-1α* significantly decreased its transcription under normoxia (Welch's t-test p = 4E-04) and hypoxia (Welch's t-test p = 0.0044) (Figure 3.15). In *HIF-1α*-silenced cells, OSM-stimulation slightly increased transcription of *HIF-1α* under normoxia and hypoxia (Figure 3.15).

In line with decreased transcription, silencing of *HIF-1α* resulted in highly reduced HIF-1α protein levels compared to the OSM-treated control under normoxia and hypoxia. I observed a minor increase in HIF-1α protein levels and increased phosphorylation of STAT3 upon OSM stimulation (Figure 3.16A, B and C).

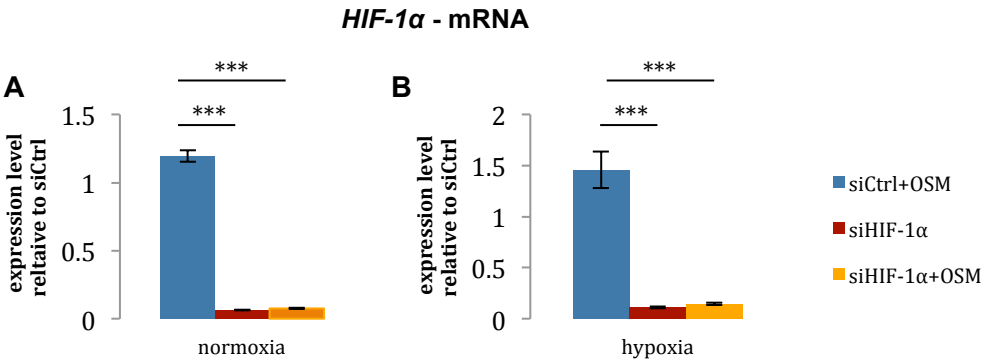

Figure 3.15 mRNA levels of *HIF-1α* relative to siCtrl under (A) normoxia and (B) hypoxia. Error bars correspond to the standard deviation of at least two independent biological replicates, Welch's t-test; *p < 0.05, **p < 0.01 and ***p < 0.001.

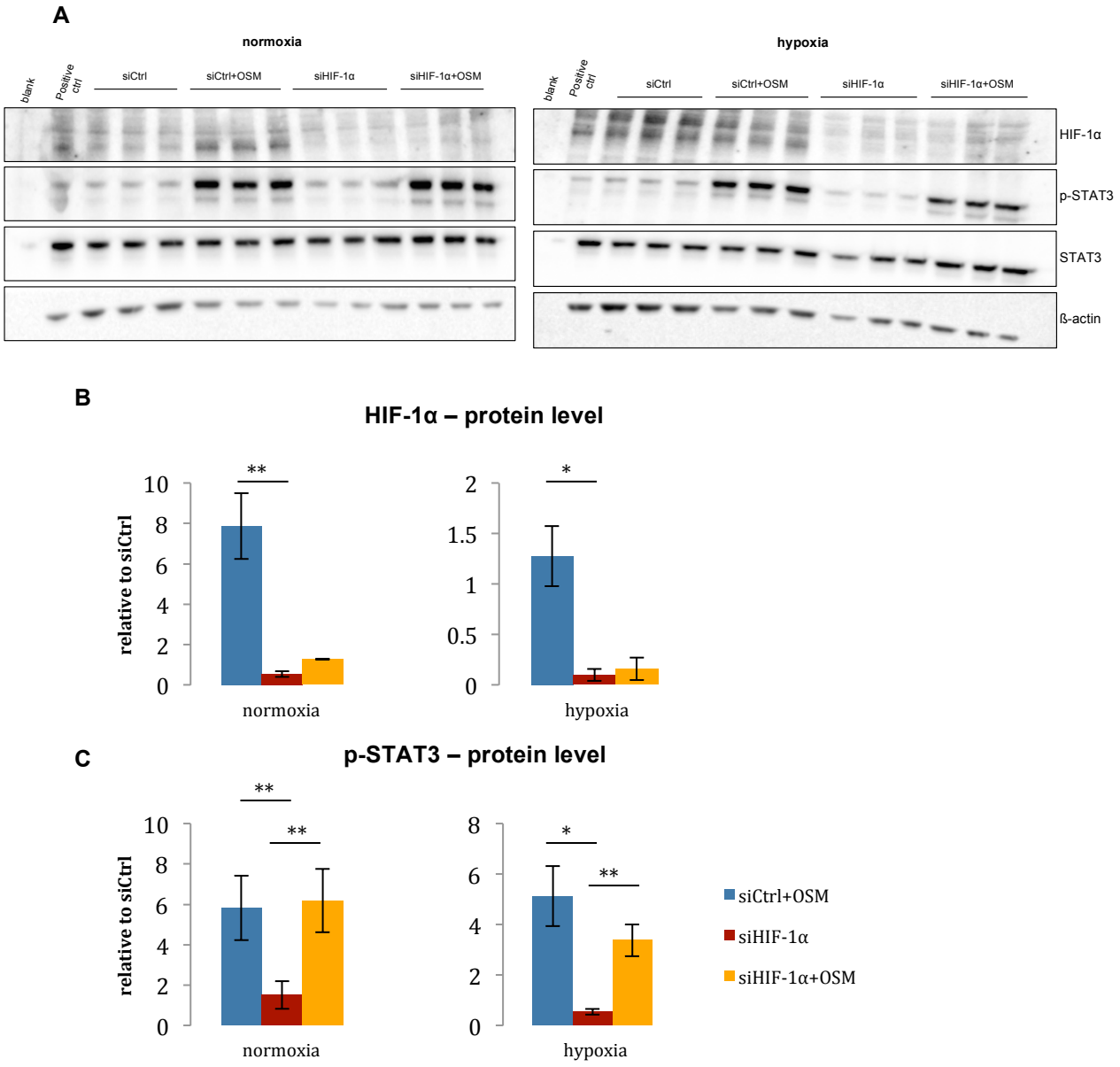

Figure 3.16 OSM stimulation results in an increase of HIF-1α protein levels under normoxia. (A) Western blot. PH5CH8 cells were treated either with OSM (siCtrl+OSM) or with DPBS (siCtrl) in normoxia or hypoxia. As positive control HeLa cells were treated with $CoCl_2$. (B)&(C) HIF-1α and phospho-STAT3 protein levels are shown relative to siCtrl in PH5CH8 cells. Protein levels of HIF-1α were normalized to ß-actin protein levels and p-STAT3 levels were normalized to STAT3. Error bars represent the standard deviation of at least two biological replicates. Welch's t-test, *p < 0.05, **p < 0.01

Next, I investigated whether HIF-1α activity is critical for OSM-induced suppression of glucose oxidation in the TCA cycle. The MIDs of citrate barely changed upon OSM stimulation in the *HIF-1α* silenced cells under normoxia (Figure 3.17A) and were comparable to the MIDs of the untreated control (A). The previously observed decreased glucose contribution to citrate upon OSM was completely impeded in the *HIF-1α* silenced cells (Figure 3.18A). Furthermore, PDH activity was not affected upon OSM-treatment in *HIF-1α* silenced cells (Figure 3.19B). In agreement with these data, OSM treatment reduced *PDK1* expression under normoxia in *HIF-1α* silenced cells (Figure 3.19A).

Under hypoxia, silencing of *HIF-1α* led to increased glucose carbon contribution to citrate (Figure 3.18B) and increased PDH activity (Figure 3.19B).

Altogether, these results strongly suggest that HIF-1α is indispensable for the OSM-mediated reprogramming of glucose oxidation via PDK1 up-regulation, and thus, PDH inhibition.

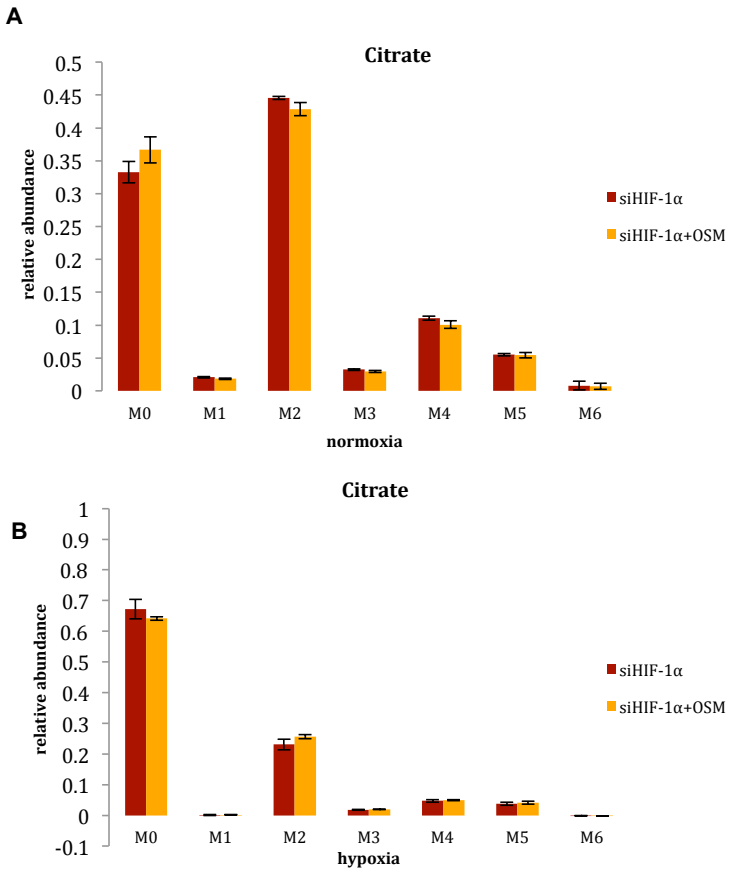

Figure 3.17 Effect of *HIF-1α* silencing on the MID of citrate from [U-$^{13}C_6$]glucose under (A) normoxia and (B) hypoxia. Error bars represent the standard deviation from at least two independent replicates (n≥2).

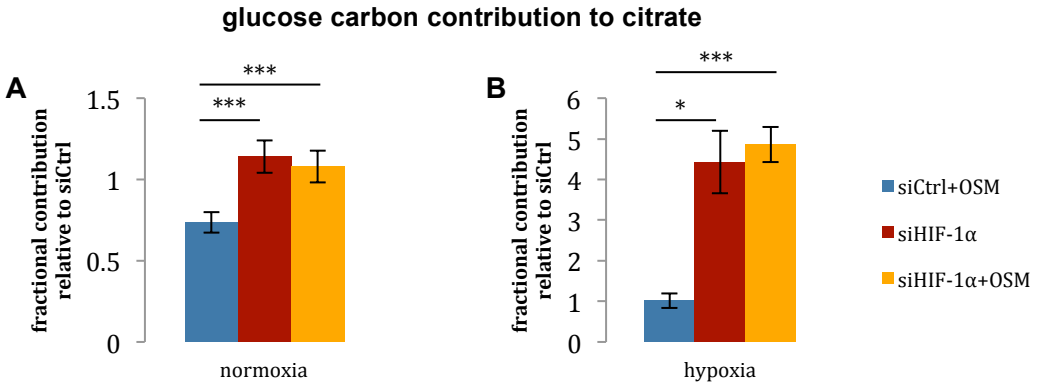

Figure 3.18 Effect of *HIF-1α* silencing on relative glucose carbon contribution to citrate under (A) normoxia and (B) hypoxia. Error bars correspond to the standard deviation of at least two independent biological replicates, Welch's t-test; *p < 0.05, **p< 0.01 and ***p < 0.001.

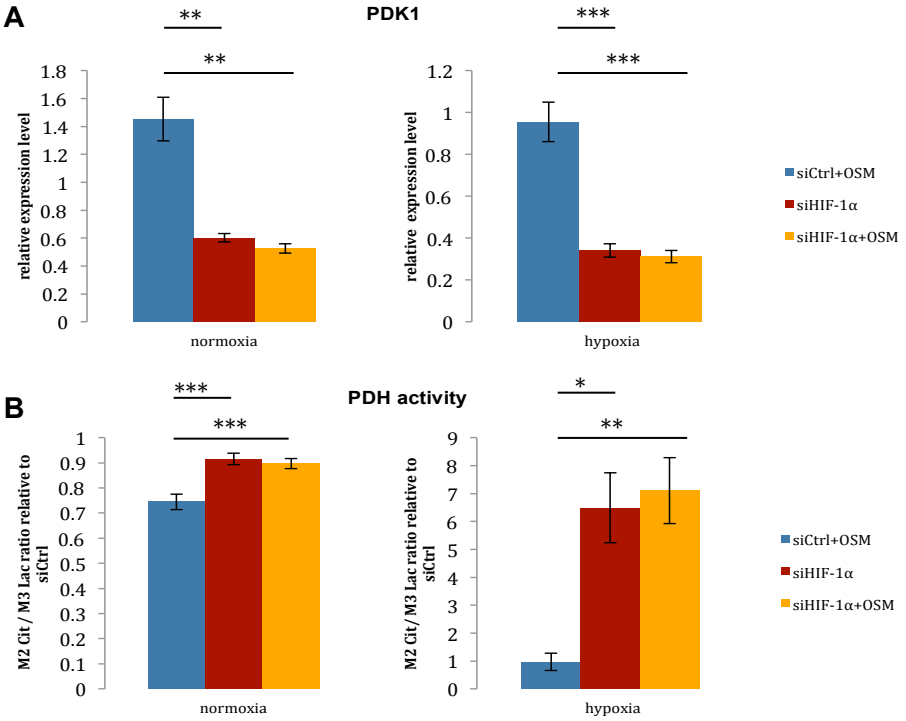

Figure 3.19 Effect of *HIF-1α* silencing on relative *PDK1* transcription and PDH activity under normoxia and hypoxia. (A) *PDK1* mRNA levels under hypoxia and normoxia. The fold change was calculated relative to the untreated control. (B) PDH activity determined by the ratio of M2 isotopologues of citrate to M3 isotopologues of lactate, from [U-$^{13}C_6$]glucose. The ratio was calculated relative to the untreated control. Error bars represent the standard deviation from at least two independent replicates (n≥2), Welch's t-test; *p < 0.05, **p < 0.01 and ***p < 0.001.

Next, I investigated the effect of *HIF-1α* silencing on glutamine metabolism. Similarly to the glucose tracer, citrate MIDs from [U-$^{13}C_5$]glutamine were not affected by OSM in *HIF-1α* silenced cells (Figure 3.20A). Silencing of *HIF-1α* almost completely prevented the OSM-induced changes in glutamine metabolism. Specifically, glutamine oxidation in the TCA cycle was only slightly decreased upon OSM stimulation in *HIF-1α* silenced cells and comparable to the untreated control (Figure 3.21A). Moreover, reductive carboxylation of α-ketoglutarate was only slightly induced by OSM treatment in *HIF-1α* silenced cells (Figure 3.22A). In line with these data, the glutamine carbon contribution to citrate was not affected by OSM treatment (Figure 3.22B).

Collectively, these data show that silencing of *HIF-1α* almost completely prevented the metabolic reprogramming induced by OSM stimulation, including suppression of glucose and glutamine oxidation via PDH inhibition, reduction of glucose and increase of glutamine carbon contribution to citrate, as well as the increase in reductive glutamine metabolism.

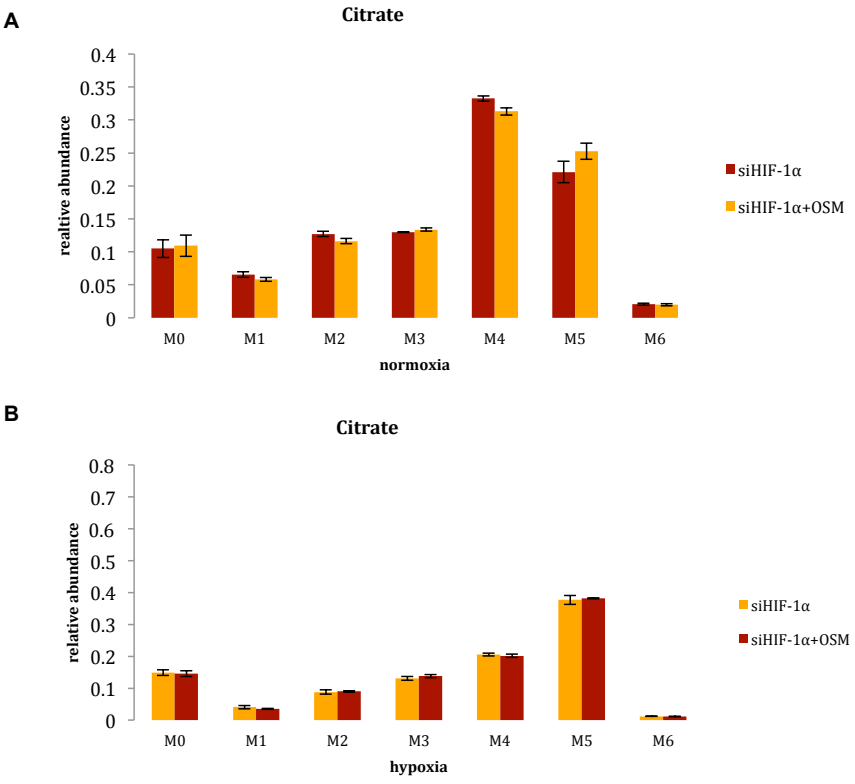

Figure 3.20 Effect of *HIF-1α* silencing on the MID of citrate from [U-$^{13}C_5$]glutamine under (A) normoxia and (B) hypoxia. Error bars represent the standard deviation from at least two independent replicates (n≥2).

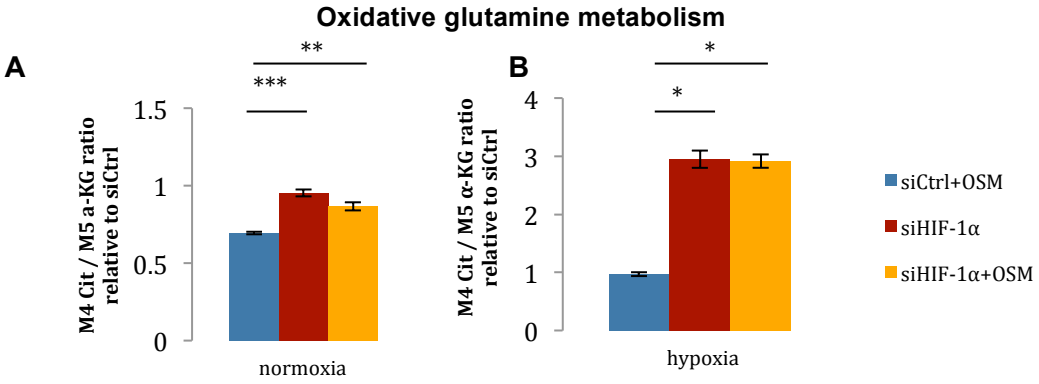

Figure 3.21 Metabolic effect of *HIF-1α* silencing on oxidative glutamine metabolism under (A) normoxia and (B) hypoxia**.** Error bars represent the standard deviation from at least two independent replicates (n≥2), Welch's t-test; *p < 0.05, **p < 0.01 and ***p < 0.001.

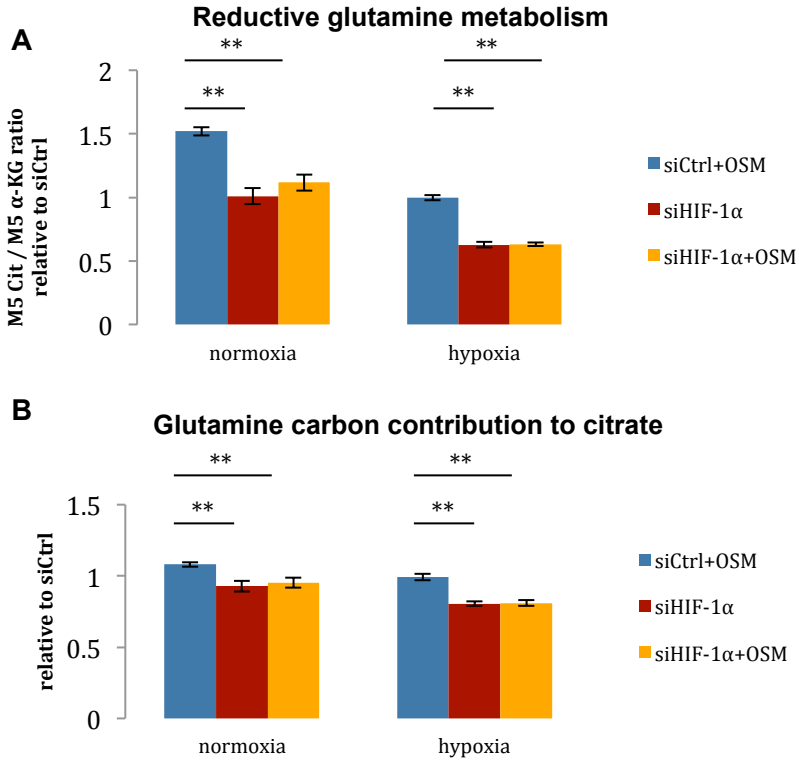

Figure 3.22 Effect of *HIF-1α* silencing on reductive glutamine metabolism and relative glutamine carbon contribution to citrate in normoxia and hypoxia from [U-$^{13}C_5$]glutamine. (A) Relative reductive glutamine metabolism, determined by the ratio of M5 isotopologues of citrate to M5 isotopologues of α-ketoglutarate. (B) Glutamine carbon contribution to citrate was calculated relative to untreated control cells. Error bars correspond to the standard deviation of at least two independent biological replicates, Welch's t-test; *p < 0.05, **p < 0.01.

In line with the results under normoxia, silencing *HIF-1α* reduced the metabolic reprogramming induced by hypoxia. Specifically, *HIF-1α* silencing led to an up-regulation of glucose and glutamine oxidation (Figure 3.21B). Moreover, silencing of *HIF-1α* increased PDH activity via PDK1 suppression, glucose carbon contribution to the TCA cycle (Figure 3.18, Figure 3.19), and decreased reductive carboxylation (Figure 3.22A). Glutamine carbon contribution to citrate decreased in *HIF-1α* silenced cells in under hypoxia (Figure 3.22B).

4 Discussion

Most tumours, which are composed of highly proliferating cells, rely on aerobic glycolysis, a phenomenon known as Warburg effect (20). Regardless the oxygen supply, these cells adapt their cellular metabolism towards a more glycolytic metabolic phenotype, by altering gene expression of crucial metabolic enzymes, which results in increased glucose uptake, high glycolytic flux, and increased lactate secretion.

Under hypoxic conditions, alterations in central carbon metabolism are mainly mediated by the transcription factor HIF-1α, a key regulator of the cellular response to hypoxia (10). Hypoxia and inflammation are often interdependent and both microenvironments have been associated with carcinogenesis (26,27). Many cancers are suggested to be preceded by chronic inflammation, indicating that inflammatory responses play a critical role at different stages of cancer development, including initiation, invasion, and metastasis (27). In particular, most hepatocellular carcinomas are preceded by chronic inflammation due to viral hepatitis infections (hepatitis B and C virus), suggesting that an inflammatory microenvironment promotes HCC development (1). IL-6-type cytokines are key regulators of this immune response, and play an important role in chronic inflammation and in the regulation of cancer development (2). Previous studies (41,42) showed that IL-6 signalling is implicated in the onset of HCC in response to chronic hepatitis B, and both liver injury and proliferation are strongly dependent on IL-6 in a mouse model (5,41,42).

In this study, I investigated the role of HIF-1α in metabolic reprogramming of human hepatocytes induced by the inflammatory cytokine OSM. Recently, it was shown that in immortalized hepatocytes and HCC cells the IL-6-type cytokine OSM up-regulates *HIF-1α* expression under normoxic conditions (8). Vollmer and colleagues showed that in response to the OSM-induced JAK/STAT3 signalling cascade, *HIF-1α* mRNA and HIF-1α protein levels are increased under normoxic conditions (21% O_2) (8). Furthermore, it was shown that STAT3 is required to increase *HIF-1α* mRNA levels in both mouse cells and human melanoma cell line (43). In line with these studies, I demonstrated that in the immortalized human hepatocyte cell line PH5CH8, *HIF-1α* transcription and protein levels are up-regulated in response to OSM. *HIF-1α* up-regulation is mediated by OSM induced activation of JAK/STAT3 signalling, where STAT3 directly acts as a transcriptional regulator of *HIF-1α* (8). Under hypoxia, *HIF-1α* transcription was enhanced upon OSM treatment, and the overall HIF-1α protein levels were increased. However, at 1% O_2 the overall *HIF-1α* mRNA levels were decreased as compared to normoxia. Uchida and colleagues showed that prolonged (>

12 hours) or acute (< 0.5 % O_2) hypoxia in the human lung adenocarcinoma cell line A549 and in human lung microvascular endothelial cells result in reduced *HIF-1α* mRNA levels (44). Thereby, HIF-1α proteins negatively regulate *HIF-1α* mRNA through an increase in natural antisense *HIF-1α* (44). In line with these findings, I observed decreased *HIF-1α* mRNA levels after 36 hours of hypoxia compared to normoxia.

OSM stimulation did not enhance HIF-1α protein levels under hypoxic conditions. These results can be explained by the different mechanisms of HIF-1α regulation. Hypoxia controls HIF-1α mainly at post-translational level (44), while OSM-induced STAT3 signalling regulates HIF-1α at transcriptional level (8,43). HIF-1α activity is mainly negatively regulated at the protein level in an oxygen-dependant manner. While HIF-1α protein is stabilized under hypoxic conditions in consequence of down-regulation of PHD activity, it is continuously degraded via prolyl hydroxylation and VHL-mediated proteasomal degradation at physiological oxygen conditions. OSM signalling, however, does not contribute to an increased HIF-1α stability, as seen under hypoxia, but induces increased transcription of *HIF-1α* (8).

Because hypoxia enhances HIF-1α protein stability, I investigated whether under normoxia OSM stimulation changes cellular metabolism towards a hypoxia-like metabolic phenotype in the human hepatocyte cell line PH5CH8.

In this thesis, I showed that OSM stimulation slightly increases glucose uptake, lactate secretion, and reduces the influx of glucose-derived carbon in the TCA cycle under normoxia. It is well known that cancer cells increase their nutrient uptake to produce essential macromolecules (e.g., nucleotides, amino acids, and lipids) to sustain rapid growth and proliferation (20). Demaria and colleagues demonstrated that lactate production and glucose uptake are significantly increased in mouse embryonic fibroblasts, expressing constitutively active STAT3 (45). In contrast to the study by Demaria and colleagues using constitutively active STAT3, I studied a transient OSM-mediated STAT3 induction that resulted only in minor increase of glucose uptake and lactate production. In addition, they showed that several known HIF-1α target genes are up-regulated in response to STAT3 signalling, including glucose transporter and two key glycolytic enzymes, phospho-fructokinase and enolase 1 (45). As a result of an increased glycolytic flux, glycolytic intermediates accumulate that are essential for the synthesis of amino acids or to fuel the pentose phosphate pathway for nucleotide synthesis and generation of reducing equivalents (20,45). For example, high glucose turnover provides ribose-5-phosphate, serine and glycine for amino acid and nucleotide synthesis (20).

Another study, done by Ando and coworkers, showed that IL-6 induced STAT3 signalling enhances glycolysis through increased expression of the glycolytic enzymes hexokinase 2

and 6-phosphofructo-2-kinase/fructose-2,6-bisphosphatase-3 in mouse embryonic fibroblasts (46).

In my work, I demonstrated that the reduced glucose carbon contribution to the TCA cycle upon OSM stimulation is mediated via reduced PDH activity. In line with decreased PDH activity, I observed increased *PDK1* expression. PDK1 is an important regulator of central carbon metabolism, because it can phosphorylate the mitochondrial PDH E1α subunit, thereby, inactivating its catalytic domain (17). In consequence, the entry of glucose-derived pyruvate into the TCA cycle is drastically decreased, thus limiting oxidative phosphorylation and promoting a higher conversion of pyruvate to lactate. These results highlight the role of PDK1 as an important enzyme, responsible for the OSM-induced metabolic phenotype. In line with these findings, Demaria and colleagues showed that in mouse embryonic fibroblasts, expressing constitutively active STAT3, *PDK1* expression is increased. As a result, mitochondrial PDH activity is reduced and the amount of pyruvate-derived acetyl-CoA entering the citric acid cycle is limited (45). Moreover, Jung-whan and colleagues showed that *PDK1* is a direct target of HIF-1α, critical for the maintenance of ATP levels and adaptation to hypoxia in MEFs and human Burkitt's lymphoma cell line (17). In order to validate PDH inhibition via *PDK1* up-regulation in response to OSM stimulation, it will be of interest to further analyse the degree of phosphorylation of PDH E1α subunit by Western Blot.

Together with a decreased PDH flux, I showed that under normoxia, glutamine oxidation was also reduced upon OSM stimulation. Decreased glutamine oxidation in combination with an increase in glutamine-derived carbon in citrate, suggested that in OSM-stimulated cells, citrate is derived from glutamine through an alternative, non-oxidative pathway. At 21% O_2 cells usually synthesize citrate through oxidation of both glucose and glutamine. Since citrate is an important metabolite required to transport acetyl-CoA from mitochondria to the cytosol for fatty acid synthesis, cancer and proliferating cells carefully adapt cellular metabolism to maintain the citrate pool for proliferation, growth and survival (26). Because citrate production from glucose-derived acetyl-CoA was drastically reduced via PDH inhibition in OSM stimulated cells, PH5CH8 cells increased synthesis of citrate through reductive carboxylation of α-ketoglutarate (47). This pathway, often called reductive flux, can synthesize citrate solely from glutamine and CO_2 without the necessity of pyruvate-derived acetyl-CoA and has been shown to be of special importance under hypoxia for lipid synthesis (18). These findings are in line with a study by Fendt and colleagues showing that as a result of reduced glucose and glutamine oxidation, the intracellular citrate levels decreased, triggering reductive α-ketoglutarate carboxylation by mass action (19).

Taken together, these data show that OSM treatment leads to increased aerobic glycolysis under normoxia (Warburg effect), characterized by an increased glucose uptake, increased

lactate production, and reduced glucose oxidation. Reduced pyruvate entry into the TCA cycle, led to increased reductive carboxylation of α-ketoglutarate, which is in line with a study by Gameiro *et al*, showing that impaired mitochondrial pyruvate oxidation triggers reductive glutamine metabolism (48). Collectively, these results highlight the importance of PDK1 as a key enzyme, responsible for the OSM-induced metabolic reprogramming.

The Warburg effect, which is characterized by high glycolytic rates and reduced glucose oxidation under normoxia, is often associated with increased cellular proliferation (20). However, I did not observe any effect of OSM stimulation on the proliferation rate of PH5CH8 cells, although I showed that OSM stimulation clearly induces a Warburg-like metabolic phenotype. PH5CH8 are immortalized human hepatocytes, and therefore proliferating cells, suggesting that the effect of OSM stimulation is not sufficient to further increase their proliferation rate. Recent studies showed that the role of IL-6 and STAT in tumour cells varies with each type of cancer (40). While cell proliferation was increased in multiple human myeloma cell lines and hepatocytes (40), cell cycle progression was inhibited in HepG2 cells in response to OSM and IL-6 signalling (49). Nevertheless, OSM-induced *HIF-1α* up-regulation, and thus, metabolic reprogramming clearly supports increased proliferation rates and might provide a selective growth advantage.

In order to investigate whether the OSM-induced metabolic reprogramming is comparable to the metabolic phenotype induced by hypoxia, I additionally examined the effect of hypoxia and OSM stimulation under hypoxia on central carbon metabolism. HIF-1α is known as a common link between adaptations to decreased O_2, cancer cell metabolism, and cancer cell progression. HIF-1α regulates metabolic enzymes and other key factors involved in glycolysis and oxidative phosphorylation under hypoxic conditions (19). Generally, hypoxia induces similar effects as OSM stimulation under normoxia, including increased glucose uptake, increased lactate production, decreased glucose and glutamine oxidation, increased *PDK1* expression and consequently decreased PDH activity, and increased reductive carboxylation of α-ketoglutarate. However, the changes induced by hypoxia were much more pronounced compared to the changes induced by OSM treatment under normoxia. Under hypoxia I did not observe any effects of OSM stimulation on central carbon metabolism. Hypoxia completely masked the effect of OSM treatment, most probably because at 1% O_2 the amount of transcriptionally active HIF-1α cannot be further induced through OSM treatment. Altogether, I demonstrated that OSM-treatment under normoxia induces an intermediate metabolic phenotype between hypoxia and normoxia in the human hepatocyte cell line PH5CH8.

Finally, I demonstrated that HIF-1α is critical for the OSM-mediated metabolic reprogramming in PH5CH8 cells. Silencing *HIF-1α* resulted in highly reduced *HIF-1α* mRNA and protein levels under normoxia and almost completely impeded the OSM-dependent suppression of glucose and glutamine oxidation. In line with these results, *HIF-1α* silencing resulted in decreased *PDK1* mRNA levels, and in consequence PDH activity was not affected by OSM-stimulation at 21% O_2. These results highlight the importance of HIF-1α as a transcriptional activator of *PDK1*, thereby indirectly regulating the activity of PDH and in consequence redirecting glucose away from oxidative phosphorylation and towards lactate production. In addition, the OSM-dependant increase of reductive glutamine metabolism was almost completely impaired in *HIF-1α* silenced cells.

Collectively, these data show that *HIF-1α* expression is critical for the OSM-dependent shift from oxidative phosphorylation to a more glycolytic metabolism.

Although O_2 supply was highly limited under hypoxia, silencing of *HIF-1α* resulted in increased glucose and glutamine oxidation. These results strongly suggest that under hypoxia PDH inhibition, and therefore, limited acetyl-CoA availability via *PDK1* up-regulation is the limiting factor for respiration and not reduced O_2 availability.

In this context, HIF-1 provides a common link between O_2 availability, cancer metabolism, and inflammation. Hypoxic and inflammatory conditions have been associated to promote cancer development by altering cellular metabolism (26,27). In particular, IL-6-type cytokines have been shown to be key players in the regulation of cancer development and progression (2). Here, I showed that aberrant OSM-mediated HIF-1α up-regulation in immortalized human hepatocytes leads to metabolic changes similar to changes induced by tumours. For this reason, cellular metabolism might provide a causal link between chronic inflammation and malignant cellular transformation. However, it is still debated whether these metabolic changes are a consequence or a cause of carcinogenesis (28).

Since HIF-1α is an important regulator of many metabolic genes, it will be of interest to further identify transcription factors downstream of HIF-1α that mediate the OSM-induced signal transduction and regulation of central carbon metabolism. Recently, it has been shown that PKM2 mediates the Warburg effect in macrophages (25). In this thesis, I did not observe a significant difference in *PKM2* expression upon OSM treatment. However, PKM2 might be regulated post-translational thereby changing its conformation (23). In the cytoplasm, PKM2 is present as tetramer and mediates the conversion of PEP to pyruvate, while in the nucleus PKM2 is a monomer and functions as kinase phosphorylating histone H3. Most probably the OSM-induced HIF-1α up-regulation under normoxia is not sufficient to increase *PKM2* transcription. In contrast to normoxia, *PKM2* transcription was increased under hypoxia, but was not affected by OSM stimulation. In hypoxic cells, HIF-1α activates *PKM2* transcription by binding to HRE. Thereby, *PKM2* mediates increased glycolytic rates and probably

enhances glucose uptake, lactate production. Recently it has been shown that PKM2 interacts with HIF-1α in the nucleus and functions as a transcriptional co-activator to stimulate the expression of HIF-1 target genes including glucose transporter 1, *LDHA*, and *PDK1* in HeLa cervical carcinoma and Hep3B hepatoblastoma cells (24).

In order to validate these findings, it would be interesting to analyse uptake and secretion rates, fluxes of central carbon metabolism and expression of glycolytic enzymes in another immortalized liver cancer cell line. As PDK1 is an important key enzyme, responsible for the OSM-induced metabolic reprogramming, it will be of interest to analyse the effect of *PDK1* knockdown in PH5CH8 cells.

Since glucose-derived acetyl-CoA is reduced upon OSM stimulation, it will be of further interest to investigate whether it is compensated by an alternative acetyl-CoA source, including fatty acid oxidation or branched chain amino acids degradation.

Cancer cells, which are highly proliferating cells, require large amounts of lipids for proliferation[21]. Therefore I would further investigate the effect of OSM and HIF-1α on fatty acid synthesis, including palmitate, a major constituent of cellular membranes.

In this thesis I studied the effect of transient OSM-induced STAT3 signalling, it will be interesting to investigate how long-term activity of the JAK/STAT3 signalling pathway or constitutively active HIF-1α affects glycolytic enzymes (e.g. GLUT, PDK1, PKM2), glucose uptake and lactate secretion and central carbon metabolism of hepatocyte under normoxic conditions.

5 References

1. European Association For The Study Of The Liver, European Organisation For Research And Treatment Of Cancer. EASL-EORTC clinical practice guidelines: management of hepatocellular carcinoma. J Hepatol. 2012 Apr;56(4):908–43.
2. Sergei Grivennikov, Michael Karin. Autocrine IL-6 Signaling: A Key Event in Tumorigenesis? Cancer Cell. 2008 Aug 1;13(1):7–9.
3. Peter C. Heinrich, Iris Behrmann, Serge Haan, Heike M. Hermanns, Gerhard Müller-Newen, Fred Schaper. Principles of interleukin (IL)-6-type cytokine signalling and its regulation. Biochem J. 2003 Aug 15;374(Pt 1):1–20.
4. P. C. Heinrich, I. Behrmann, G. Müller-Newen, F. Schaper, L. Graeve. Interleukin-6-type cytokine signalling through the gp130/Jak/STAT pathway. Biochem J. 1998 Sep 1;334 (Pt 2):297–314.
5. Yan Liu, James Fuchs, Chenglong Li, Jiayuh Lin. IL-6, a risk factor for hepatocellular carcinoma: FLLL32 inhibits IL-6-induced STAT3 phosphorylation in human hepatocellular cancer cells. Cell Cycle Georget Tex. 2010 Sep 1;9(17):3423–7.
6. Kodappully Sivaraman Siveen, Sakshi Sikka, Rohit Surana, Xiaoyun Dai, Jingwen Zhang, Alan Prem Kumar, et al. Targeting the STAT3 signaling pathway in cancer: role of synthetic and natural inhibitors. Biochim Biophys Acta. 2014 Apr;1845(2):136–54.
7. Bharat B. Aggarwal, Ajaikumar B. Kunnumakkara, Kuzhuvelil B. Harikumar, Shan R. Gupta, Sheeja T. Tharakan, Cemile Koca, et al. Signal transducer and activator of transcription-3, inflammation, and cancer: how intimate is the relationship? Ann N Y Acad Sci. 2009 Aug;1171:59–76.
8. Stefan Vollmer, Valérie Kappler, Jakub Kaczor, Daniela Flügel, Catherine Rolvering, Nobuyuki Kato. Hypoxia-inducible factor 1alpha is up-regulated by oncostatin M and participates in oncostatin M signaling. Hepatol Baltim Md. 2009 Jul;50(1):253–60.
9. L. E. Huang, J. Gu, M. Schau, H. F. Bunn. Regulation of hypoxia-inducible factor 1alpha is mediated by an O2-dependent degradation domain via the ubiquitin-proteasome pathway. Proc Natl Acad Sci U S A. 1998 Jul 7;95(14):7987–92.
10. Vera Mucaj, Jessica E. S. Shay, M. Celeste Simon. Effects of hypoxia and HIFs on cancer metabolism. Int J Hematol. 2012 May;95(5):464–70.
11. Ekaterina Moroz, Sean Carlin, Katerina Dyomina, Sean Burke, Howard T. Thaler, Ronald Blasberg, et al. Real-time imaging of HIF-1alpha stabilization and degradation. PloS One. 2009;4(4):e5077.
12. Hewitson KS, Liénard BMR, McDonough MA, Clifton IJ, Butler D, Soares AS, et al. Structural and mechanistic studies on the inhibition of the hypoxia-inducible transcription factor hydroxylases by tricarboxylic acid cycle intermediates. J Biol Chem. 2007 Feb 2;282(5):3293–301.
13. Dewi Astuti, Christopher J. Ricketts, Rasheduzzaman Chowdhury, Michael A. McDonough, Dean Gentle, Gail Kirby, et al. Mutation analysis of HIF prolyl hydroxylases (PHD/EGLN) in individuals with features of phaeochromocytoma and renal cell carcinoma susceptibility. Endocr Relat Cancer. 2011 Feb;18(1):73–83.
14. Elizabeth C. Finger, Amato J. Giaccia. Hypoxia, inflammation, and the tumor microenvironment in metastatic disease. Cancer Metastasis Rev. 2010 Jun;29(2):285–93.
15. G. L. Semenza. HIF-1: mediator of physiological and pathophysiological responses to hypoxia. J Appl Physiol Bethesda Md 1985. 2000 Apr;88(4):1474–80.
16. Ioanna Papandreou, Rob A. Cairns, Lucrezia Fontana, Ai Lin Lim, Nicholas C. Denko. HIF-1 mediates adaptation to hypoxia by actively downregulating mitochondrial oxygen consumption. Cell Metab. 2006 Mar;3(3):187–97.
17. Jung-whan Kim, Irina Tchernyshyov, Gregg L. Semenza, Chi V. Dang. HIF-1-mediated expression of pyruvate dehydrogenase kinase: a metabolic switch required for cellular adaptation to hypoxia. Cell Metab. 2006 Mar;3(3):177–85.

18. Christian M. Metallo, Paulo A. Gameiro, Eric L. Bell, Katherine R. Mattaini, Juanjuan Yang, Karsten Hiller, et al. Reductive glutamine metabolism by IDH1 mediates lipogenesis under hypoxia. Nature. 2012 Jan 19;481(7381):380–4.
19. Sarah-Maria Fendt, Eric L. Bell, Mark A. Keibler, Benjamin A. Olenchock, Jared R. Mayers, Thomas M. Wasylenko, et al. Reductive glutamine metabolism is a function of the α-ketoglutarate to citrate ratio in cells. Nat Commun. 2013;4:2236.
20. Matthew G. Vander Heiden, Lewis C. Cantley, Craig B. Thompson. Understanding the Warburg effect: the metabolic requirements of cell proliferation. Science. 2009 May 22;324(5930):1029–33.
21. David R. Wise, Patrick S. Ward, Jessica E. S. Shay, Justin R. Cross, Joshua J. Gruber, Uma M. Sachdeva, et al. Hypoxia promotes isocitrate dehydrogenase-dependent carboxylation of α-ketoglutarate to citrate to support cell growth and viability. Proc Natl Acad Sci U S A. 2011 Dec 6;108(49):19611–6.
22. Lehninger Principles of Biochemistry. 5th edition. New York, NY: W. H. Freeman; 2008. 1100 p.
23. Weiwei Yang, Zhimin Lu. Nuclear PKM2 regulates the Warburg effect. Cell Cycle Georget Tex. 2013 Oct 1;12(19):3154–8.
24. Weibo Luo, Gregg L. Semenza. Emerging roles of PKM2 in cell metabolism and cancer progression. Trends Endocrinol Metab TEM. 2012 Nov;23(11):560–6.
25. Eva M. Palsson-McDermott, Anne M. Curtis, Gautam Goel, Mario A. R. Lauterbach, Frederick J. Sheedy, Laura E. Gleeson, et al. Pyruvate kinase M2 regulates Hif-1α activity and IL-1β induction and is a critical determinant of the warburg effect in LPS-activated macrophages. Cell Metab. 2015 Jan 6;21(1):65–80.
26. Douglas Hanahan, Robert A. Weinberg. Hallmarks of cancer: the next generation. Cell. 2011 Mar 4;144(5):646–74.
27. Sergei I. Grivennikov, Florian R. Greten, Michael Karin. Immunity, Inflammation, and Cancer. Cell. 2010 Mar 19;140(6):883–99.
28. Russell G. Jones, Craig B. Thompson. Tumor suppressors and cell metabolism: a recipe for cancer growth. Genes Dev. 2009 Mar 1;23(5):537–48.
29. Wegner A. Computational Tools for Mass Spectrometry Based Metabolic Profiling. 2013 Dec 13 [cited 2015 Apr 19]; Available from: http://orbilu.uni.lu/handle/10993/16491
30. Chokkathukalam A, Kim D-H, Barrett MP, Breitling R, Creek DJ. Stable isotope-labeling studies in metabolomics: new insights into structure and dynamics of metabolic networks. Bioanalysis. 2014 Feb;6(4):511–24.
31. Sebastian Klein, Elmar Heinzle. Isotope labeling experiments in metabolomics and fluxomics. Wiley Interdiscip Rev Syst Biol Med. 2012 Jun;4(3):261–72.
32. Andre Wegner, Thekla Cordes, Alessandro Michelucci, Karsten Hiller. The Application of Stable Isotope Assisted Metabolomics in Biomedicine. Curr Biotechnol E. 2012 Feb 1;1(1):88–97.
33. Dajana Vuckovic. Current trends and challenges in sample preparation for global metabolomics using liquid chromatography-mass spectrometry. Anal Bioanal Chem. 2012 Jun;403(6):1523–48.
34. O. Hernández-Hernández A I Ruiz-Matute. Derivatization of carbohydrates for GC and GC-MS analyses. J Chromatogr B Analyt Technol Biomed Life Sci. 2010;879(17-18):1226–40.
35. André Wegner, Sean C. Sapcariu, Daniel Weindl, Karsten Hiller. Isotope cluster-based compound matching in gas chromatography/mass spectrometry for non-targeted metabolomics. Anal Chem. 2013 Apr 16;85(8):4030–7.
36. Mark E. Jennings, Dwight E. Matthews. Determination of complex isotopomer patterns in isotopically labeled compounds by mass spectrometry. Anal Chem. 2005 Oct 1;77(19):6435–44.
37. Daniel Mueller, Elmar Heinzle. Stable isotope-assisted metabolomics to detect metabolic flux changes in mammalian cell cultures. Curr Opin Biotechnol. 2013 Feb;24(1):54–9.
38. André Wegner, Daniel Weindl, Christian Jäger, Sean C. Sapcariu, Xiangyi Dong, Gregory Stephanopoulos, et al. Fragment Formula Calculator (FFC): Determination of

Chemical Formulas for Fragment Ions in Mass Spectrometric Data. Anal Chem. 2014 Feb 18;86(4):2221–8.
39. Karsten Hiller, Jasper Hangebrauk, Christian Jäger, Jana Spura, Kerstin Schreiber, Dietmar Schomburg. MetaboliteDetector: comprehensive analysis tool for targeted and nontargeted GC/MS based metabolome analysis. Anal Chem. 2009 May 1;81(9):3429–39.
40. David R. Hodge, Elaine M. Hurt, William L. Farrar. The role of IL-6 and STAT3 in inflammation and cancer. Eur J Cancer Oxf Engl 1990. 2005 Nov;41(16):2502–12.
41. Willscott E. Naugler, Toshiharu Sakurai, Sunhwa Kim, Shin Maeda, KyoungHyun Kim, Ahmed M. Elsharkawy, et al. Gender Disparity in Liver Cancer Due to Sex Differences in MyD88-Dependent IL-6 Production. Science. 2007 Jul 6;317(5834):121–4.
42. Vincent Wai-Sun Wong, Jun Yu, Alfred Sze-Lok Cheng, Grace Lai-Hung Wong, Hoi-Yun Chan, Eagle Siu-Hong Chu, et al. High serum interleukin-6 level predicts future hepatocellular carcinoma development in patients with chronic hepatitis B. Int J Cancer J Int Cancer. 2009 Jun 15;124(12):2766–70.
43. Guilian Niu, Jon Briggs, Jiehui Deng, Yihong Ma. Signal Transducer and Activator of Transcription 3 is required for hypoxia-inducible factor-1α RNA expression in both tumor cells and tumor-associated myeloid cells. Mol Cancer Res MCR. 2008 Jul;6(7):1099–105.
44. Tokujiro Uchida, Fabrice Rossignol, Michael A. Matthay, Rémi Mounier, Sylvianne Couette, Eric Clottes, et al. Prolonged hypoxia differentially regulates hypoxia-inducible factor (HIF)-1alpha and HIF-2alpha expression in lung epithelial cells: implication of natural antisense HIF-1alpha. J Biol Chem. 2004 Apr 9;279(15):14871–8.
45. Marco Demaria, Carlotta Giorgi, Magdalena Lebiedzinska, Giovanna Esposito, Luca D'Angeli, Antonietta Bartoli, et al. A STAT3-mediated metabolic switch is involved in tumour transformation and STAT3 addiction. Aging. 2010 Nov;2(11):823–42.
46. Masaru Ando, Ikuno Uehara, Kayo Kogure. Interleukin 6 enhances glycolysis through expression of the glycolytic enzymes hexokinase 2 and 6-phosphofructo-2-kinase/fructose-2,6-bisphosphatase-3. J Nippon Med Sch Nippon Ika Daigaku Zasshi. 2010 Apr;77(2):97–105.
47. Andre Wegner, Johannes Meiser, Daniel Weindl, Karsten Hiller. How metabolites modulate metabolic flux. Curr Opin Biotechnol. 2015 Aug;34:16–22.
48. Paulo A. Gameiro, Juanjuan Yang, Ana M. Metelo, Rocio Pérez-Carro, Rania Baker, Zongwei Wang, et al. In Vivo HIF-Mediated Reductive Carboxylation Is Regulated by Citrate Levels and Sensitizes VHL-Deficient Cells to Glutamine Deprivation. Cell Metab. 2013 Mar 5;17(3):372–85.
49. P. Klausen, L. Pedersen, J. Jurlander, H. Baumann. Oncostatin M and interleukin 6 inhibit cell cycle progression by prevention of p27kip1 degradation in HepG2 cells. Oncogene. 2000 Jul 27;19(32):3675–83.

6 Appendix

Supplemental Table 1. MID from [U-$^{13}C_6$]glucose under normoxia.

Metabolites	mass isotopomers	siCtrl average	siCtrl stdev	siCtrl+OSM average	siCtrl+OSM stdev	siHIF-1α average	siHIF-1α stdev	siHIF-1α+OSM average	siHIF-1α+OSM stdev
Malate_419	M0	0,8310	0,0183	0,8739	0,0068	0,7713	0,0082	0,7896	0,0094
	M1	0,0130	0,0021	0,0061	0,0010	0,0182	0,0008	0,0151	0,0010
	M2	0,1079	0,0100	0,0705	0,0045	0,1341	0,0045	0,1227	0,0043
	M3	0,0435	0,0050	0,0465	0,0009	0,0647	0,0022	0,0626	0,0034
	M4	0,0051	0,0011	0,0034	0,0004	0,0121	0,0006	0,0105	0,0008
Pyruvate_174	M0	0,1161	0,0217	0,1900	0,1582	0,1539	0,0224	0,0909	0,0202
	M1	0,0101	0,0027	0,0069	0,0028	0,0111	0,0024	0,0051	0,0005
	M2	0,0353	0,0009	0,0319	0,0062	0,0348	0,0014	0,0356	0,0007
	M3	0,8429	0,0232	0,7754	0,1502	0,8045	0,0226	0,8727	0,0202
Glutamate_432	M0	0,8533	0,0075	0,8995	0,0204	0,7757	0,0030	0,7098	0,2479
	M1	0,0067	0,0012	0,0034	0,0005	0,0092	0,0007	0,0933	0,1471
	M2	0,1273	0,0161	0,0899	0,0070	0,1535	0,0061	0,1838	0,0566
	M3	0,0140	0,0026	0,0077	0,0008	0,0254	0,0011	0,0185	0,0080
	M4	-0,0035	0,0297	-0,0021	0,0208	0,0307	0,0008	-0,0135	0,0469
	M5	0,0031	0,0007	0,0026	0,0005	0,0087	0,0019	0,0073	0,0067
Succinate_289	M0	0,8941	0,0239	0,9201	0,0022	0,8445	0,0061	0,8574	0,0252
	M1	0,0016	0,0019	-0,0005	0,0004	0,0060	0,0006	0,0046	0,0020
	M2	0,0826	0,0149	0,0642	0,0020	0,1061	0,0050	0,0994	0,0170
	M3	0,0162	0,0045	0,0099	0,0008	0,0307	0,0016	0,0271	0,0053
	M4	0,0073	0,0028	0,0071	0,0014	0,0143	0,0011	0,0130	0,0012
Serine_390	M0	0,8277	0,0142	0,8266	0,0062	0,8677	0,0074	0,8771	0,0065
	M1	0,0481	0,0060	0,0464	0,0020	0,0301	0,0027	0,0286	0,0022
	M2	0,0285	0,0029	0,0262	0,0011	0,0193	0,0014	0,0173	0,0012
	M3	0,0969	0,0053	0,1021	0,0034	0,0840	0,0033	0,0779	0,0033
Lactate_261	M0	0,0750	0,0208	0,0571	0,0059	0,0698	0,0114	0,0858	0,0261
	M1	0,0031	0,0002	0,0028	0,0000	0,0035	0,0002	0,0030	0,0003
	M2	0,0395	0,0011	0,0402	0,0004	0,0404	0,0005	0,0398	0,0012
	M3	0,8851	0,0191	0,9022	0,0056	0,8891	0,0108	0,8729	0,0245
Fumarate_287	M0	0,8379	0,0176	0,8754	0,0045	0,7897	0,0100	0,8072	0,0101
	M1	0,0251	0,0067	0,0176	0,0032	0,0314	0,0046	0,0265	0,0033
	M2	0,0940	0,0124	0,0629	0,0059	0,1127	0,0104	0,1070	0,0094
	M3	0,0388	0,0051	0,0413	0,0008	0,0555	0,0035	0,0506	0,0025
	M4	0,0052	0,0015	0,0037	0,0001	0,0125	0,0009	0,0097	0,0012
Glycine_246	M0	0,9305	0,0077	0,9317	0,0099	0,9453	0,0035	0,9504	0,0062
	M1	0,0007	0,0005	0,0010	0,0003	-0,0003	0,0002	-0,0001	0,0005
	M2	0,0692	0,0071	0,0675	0,0097	0,0553	0,0034	0,0501	0,0057
a-Ketoglutarate_346	M0	0,8468	0,0200	0,8945	0,0095	0,7916	0,0079	0,8099	0,0098
	M1	0,0039	0,0013	0,0007	0,0006	0,0064	0,0002	0,0053	0,0005
	M2	0,1181	0,0126	0,0853	0,0066	0,1420	0,0051	0,1314	0,0059
	M3	0,0128	0,0026	0,0072	0,0009	0,0226	0,0012	0,0197	0,0014
	M4	0,0155	0,0028	0,0098	0,0010	0,0296	0,0014	0,0267	0,0017
	M5	0,0035	0,0009	0,0029	0,0003	0,0091	0,0005	0,0081	0,0007
Citric acid_591	M0	0,3603	0,0286	0,5258	0,0127	0,3327	0,0162	0,3666	0,0198
	M1	0,0205	0,0011	0,0111	0,0004	0,0206	0,0011	0,0184	0,0012
	M2	0,4845	0,0074	0,3676	0,0074	0,4455	0,0025	0,4287	0,0100
	M3	0,0200	0,0027	0,0149	0,0003	0,0323	0,0013	0,0292	0,0016
	M4	0,0830	0,0078	0,0511	0,0032	0,1107	0,0031	0,1007	0,0057
	M5	0,0338	0,0044	0,0286	0,0013	0,0552	0,0020	0,0540	0,0039
	M6	0,0016	0,0045	0,0029	0,0008	0,0080	0,0068	0,0069	0,0046
Aspartate_418	M0	0,8284	0,0175	0,8762	0,0083	0,7729	0,0081	0,7939	0,0072
	M1	0,0144	0,0017	0,0069	0,0010	0,0196	0,0008	0,0165	0,0007
	M2	0,1100	0,0097	0,0704	0,0050	0,1355	0,0041	0,1252	0,0041
	M3	0,0420	0,0051	0,0429	0,0019	0,0602	0,0027	0,0541	0,0020
	M4	0,0054	0,0011	0,0039	0,0004	0,0121	0,0006	0,0106	0,0005
Methionine_320	M0	0,9989	0,0013	0,9978	0,0003	0,9999	0,0015	1,0020	0,0085
	M1	-0,0036	0,0007	-0,0030	0,0004	-0,0039	0,0006	-0,0035	0,0007
	M2	-0,0008	0,0001	-0,0010	0,0003	-0,0007	0,0003	-0,0005	0,0000
	M3	-0,0002	0,0003	-0,0002	0,0003	-0,0004	0,0002	-0,0004	0,0009
	M4	0,0090	0,0007	0,0098	0,0007	0,0081	0,0007	0,0044	0,0096
	M5	-0,0030	0,0002	-0,0032	0,0002	-0,0028	0,0002	-0,0019	0,0023

Supplemental Table 2. MID from [U-$^{13}C_5$]glutamine under normoxia.

Metabolites	mass isotopomers	siCtrl average	siCtrl stdev	siCtrl+OSM average	siCtrl+OSM stdev	siHIF-1α average	siHIF-1α stdev	siHIF-1α+OSM average	siHIF-1α+OSM stdev
Malate_419	M0	0,0711	0,0024	0,0883	0,0022	0,0932	0,0053	0,0897	0,0061
	M1	0,0407	0,0023	0,0255	0,0001	0,0572	0,0055	0,0484	0,0025
	M2	0,1356	0,0036	0,1093	0,0002	0,1492	0,0073	0,1383	0,0034
	M3	0,1849	0,0023	0,2609	0,0008	0,1554	0,0034	0,1774	0,0027
	M4	0,5749	0,0060	0,5229	0,0026	0,5520	0,0150	0,5531	0,0098
Pyruvate_174	M0	0,9750	0,0015	0,9811	0,0016	0,9734	0,0024	0,9780	0,0038
	M1	0,0022	0,0007	0,0012	0,0005	0,0057	0,0031	0,0044	0,0036
	M2	0,0044	0,0003	0,0038	0,0003	0,0045	0,0003	0,0037	0,0003
	M3	0,0190	0,0010	0,0142	0,0008	0,0176	0,0004	0,0148	0,0015
Glutamate_432	M0	0,0574	0,0298	0,0793	0,0332	0,0508	0,0046	0,0635	0,0278
	M1	0,0367	0,0174	0,0492	0,0206	0,0371	0,0047	0,0405	0,0164
	M2	0,0390	0,0134	0,0466	0,0195	0,0433	0,0034	0,0441	0,0104
	M3	0,1063	0,0431	0,0731	0,0205	0,1472	0,0080	0,1083	0,0424
	M4	0,0481	0,0072	0,0415	0,0041	0,0398	0,0004	0,0474	0,0101
	M5	0,7240	0,0283	0,7218	0,0589	0,6878	0,0204	0,7078	0,0259
Succinate_289	M0	0,4249	0,0514	0,3342	0,0460	0,3766	0,0533	0,3727	0,0316
	M1	0,0173	0,0007	0,0125	0,0008	0,0313	0,0046	0,0272	0,0034
	M2	0,0818	0,0053	0,0743	0,0044	0,1003	0,0087	0,0934	0,0070
	M3	0,0238	0,0024	0,0270	0,0021	0,0248	0,0018	0,0248	0,0010
	M4	0,4549	0,0438	0,5556	0,0391	0,4718	0,0459	0,4846	0,0211
Serine_390	M0	1,0064	0,0005	1,0066	0,0005	1,0070	0,0001	1,0067	0,0004
	M1	-0,0051	0,0004	-0,0051	0,0003	-0,0054	0,0002	-0,0053	0,0001
	M2	-0,0012	0,0001	-0,0013	0,0002	-0,0014	0,0002	-0,0012	0,0002
	M3	0,0000	0,0001	0,0000	0,0000	-0,0001	0,0001	0,0000	0,0001
Lactate_261	M0	0,9776	0,0006	0,9840	0,0004	0,9825	0,0006	0,9833	0,0015
	M1	0,0012	0,0004	0,0009	0,0002	0,0000	0,0005	0,0009	0,0009
	M2	0,0047	0,0001	0,0038	0,0001	0,0038	0,0003	0,0038	0,0004
	M3	0,0169	0,0001	0,0116	0,0002	0,0139	0,0003	0,0123	0,0003
Fumarate_287	M0	0,1384	0,0036	0,1194	0,0011	0,1563	0,0073	0,1476	0,0040
	M1	0,1043	0,0027	0,0900	0,0008	0,1178	0,0055	0,1113	0,0030
	M2	0,0984	0,0025	0,0849	0,0008	0,1111	0,0052	0,1050	0,0028
	M3	0,1583	0,0030	0,2288	0,0004	0,1346	0,0042	0,1528	0,0027
	M4	0,5009	0,0056	0,4776	0,0021	0,4803	0,0138	0,4839	0,0081
Glycine_246	M0	1,0013	0,0004	1,0007	0,0001	1,0024	0,0005	1,0016	0,0001
	M1	-0,0021	0,0002	-0,0016	0,0001	-0,0028	0,0003	-0,0023	0,0002
	M2	0,0010	0,0002	0,0011	0,0001	0,0006	0,0002	0,0009	0,0001
a-Ketoglutarate_346	M0	0,0299	0,0016	0,0311	0,0006	0,0454	0,0037	0,0432	0,0016
	M1	0,0190	0,0015	0,0113	0,0001	0,0310	0,0043	0,0254	0,0019
	M2	0,0324	0,0015	0,0276	0,0002	0,0399	0,0034	0,0361	0,0016
	M3	0,1186	0,0040	0,0868	0,0007	0,1321	0,0090	0,1179	0,0041
	M4	0,0403	0,0003	0,0416	0,0000	0,0377	0,0007	0,0389	0,0005
	M5	0,7651	0,0079	0,8071	0,0013	0,7188	0,0199	0,7441	0,0088
Citric acid_591	M0	0,0723	0,0012	0,0811	0,0059	0,1050	0,0136	0,1095	0,0163
	M1	0,0419	0,0015	0,0281	0,0004	0,0655	0,0041	0,0581	0,0030
	M2	0,1118	0,0022	0,0840	0,0003	0,1271	0,0042	0,1162	0,0040
	M3	0,1453	0,0012	0,1456	0,0014	0,1299	0,0006	0,1338	0,0022
	M4	0,3716	0,0041	0,2720	0,0023	0,3327	0,0040	0,3130	0,0056
	M5	0,2325	0,0056	0,3727	0,0018	0,2210	0,0162	0,2527	0,0123
	M6	0,0284	0,0006	0,0187	0,0001	0,0208	0,0016	0,0199	0,0017
Aspartate_418	M0	0,0728	0,0027	0,0933	0,0025	0,0905	0,0062	0,0863	0,0052
	M1	0,0424	0,0024	0,0266	0,0003	0,0587	0,0052	0,0503	0,0025
	M2	0,1394	0,0032	0,1104	0,0003	0,1525	0,0064	0,1421	0,0032
	M3	0,1842	0,0022	0,2557	0,0000	0,1541	0,0030	0,1740	0,0020
	M4	0,5675	0,0060	0,5199	0,0023	0,5501	0,0149	0,5535	0,0092
Methionine_320	M0	1,0094	0,0036	1,0061	0,0006	1,0104	0,0030	1,0069	0,0010
	M1	-0,0039	0,0004	-0,0034	0,0006	-0,0043	0,0005	-0,0040	0,0002
	M2	-0,0004	0,0001	-0,0010	0,0000	-0,0011	0,0006	-0,0006	0,0004
	M3	-0,0010	0,0005	-0,0008	0,0001	-0,0010	0,0003	-0,0013	0,0008
	M4	-0,0046	0,0038	-0,0002	0,0000	-0,0046	0,0037	-0,0004	0,0002
	M5	0,0002	0,0009	-0,0008	0,0000	0,0002	0,0009	-0,0007	0,0002

Supplemental Table 3. MID from [U-$^{13}C_6$]glucose under hypoxia.

Metabolites	mass isotopomers	siCtrl average	siCtrl stdev	siCtrl+OSM average	siCtrl+OSM stdev	siHIF-1α average	siHIF-1α stdev	siHIF-1α+OSM average	siHIF-1α+OSM stdev
Malate_419	M0	0,9004	0,0089	0,8671	0,0235	0,8471	0,0006	0,8391	0,0017
	M1	-0,0042	0,0003	-0,0045	0,0007	0,0050	0,0009	0,0046	0,0011
	M2	0,0188	0,0014	0,0206	0,0003	0,0669	0,0039	0,0686	0,0027
	M3	0,0866	0,0109	0,1195	0,0253	0,0782	0,0052	0,0850	0,0025
	M4	-0,0005	0,0004	-0,0008	0,0004	0,0045	0,0009	0,0045	0,0003
Lactate_261	M0	0,0481	0,0037	0,0439	0,0081	0,0616	0,0177	0,0468	0,0032
	M1	0,0016	0,0000	0,0016	0,0001	0,0019	0,0001	0,0019	0,0001
	M2	0,0308	0,0003	0,0315	0,0005	0,0305	0,0008	0,0310	0,0001
	M3	0,9201	0,0043	0,9229	0,0074	0,9068	0,0162	0,9210	0,0030
Methionine_320	M0	1,0054	0,0006	1,0042	0,0001	1,0104	0,0059	1,0065	0,0008
	M1	-0,0049	0,0003	-0,0041	0,0002	-0,0098	0,0067	-0,0057	0,0013
	M2	-0,0011	0,0002	-0,0009	0,0003	-0,0008	0,0006	-0,0011	0,0005
	M3	-0,0003	0,0003	-0,0002	0,0001	-0,0002	0,0002	-0,0002	0,0001
	M4	0,0023	0,0004	0,0025	0,0005	0,0015	0,0001	0,0018	0,0002
	M5	-0,0015	0,0001	-0,0015	0,0001	-0,0013	0,0000	-0,0013	0,0000
Succinate_289	M0	0,9910	0,0037	0,9858	0,0011	0,9393	0,0123	0,9275	0,0059
	M1	-0,0041	0,0005	-0,0028	0,0005	0,0006	0,0008	0,0004	0,0007
	M2	0,0063	0,0029	0,0056	0,0019	0,0396	0,0067	0,0449	0,0049
	M3	0,0008	0,0004	0,0008	0,0003	0,0097	0,0016	0,0103	0,0009
	M4	0,0077	0,0007	0,0136	0,0035	0,0131	0,0017	0,0186	0,0005
Pyruvate_174	M0	0,0974	0,0110	0,0766	0,0140	0,0956	0,0068	0,1043	0,0065
	M1	0,0005	0,0000	0,0006	0,0000	0,0010	0,0001	0,0009	0,0002
	M2	0,0274	0,0001	0,0280	0,0003	0,0277	0,0003	0,0273	0,0001
	M3	0,8789	0,0107	0,8987	0,0135	0,8797	0,0065	0,8719	0,0066
Fumarate_287	M0	0,9483	0,0066	0,9456	0,0070	0,9316	0,0042	0,9457	
	M1	0,0144	0,0030	0,0133	0,0028	0,0203	0,0011	0,0124	
	M2	0,0046	0,0025	0,0032	0,0057	0,0301	0,0034	0,0236	
	M3	0,0467	0,0046	0,0534	0,0055	0,0303	0,0029	0,0300	
	M4	-0,0132	0,0012	-0,0145	0,0016	-0,0121	0,0009	-0,0114	
Glycine_246	M0	0,9581	0,0056	0,9588	0,0059	0,9681	0,0006	0,9688	0,0011
	M1	-0,0001	0,0002	0,0001	0,0001	-0,0009	0,0001	-0,0008	0,0000
	M2	0,0423	0,0056	0,0414	0,0058	0,0330	0,0007	0,0325	0,0008
Glutamate_432	M0	0,9778	0,0018	0,9767	0,0032	0,8813	0,0023	0,8582	0,0029
	M1	0,0037	0,0004	0,0033	0,0003	0,0058	0,0001	0,0063	0,0004
	M2	0,0161	0,0021	0,0155	0,0024	0,0923	0,0040	0,1008	0,0045
	M3	0,0025	0,0001	0,0027	0,0002	0,0137	0,0011	0,0147	0,0011
	M4	0,0011	0,0001	0,0013	0,0002	0,0159	0,0010	0,0164	0,0006
	M5	-0,0016	0,0019	0,0008	0,0001	-0,0112	0,0019	0,0056	0,0014
Aspartate_418	M0	0,9197	0,0033	0,8954	0,0062	0,8704	0,0075	0,8611	0,0010
	M1	-0,0028	0,0005	-0,0027	0,0005	0,0073	0,0008	0,0070	0,0005
	M2	0,0192	0,0015	0,0209	0,0009	0,0706	0,0037	0,0737	0,0014
	M3	0,0595	0,0027	0,0734	0,0010	0,0426	0,0040	0,0473	0,0021
	M4	0,0052	0,0015	0,0144	0,0071	0,0100	0,0011	0,0118	0,0013
Citric acid_591	M0	0,9685	0,0045	0,9685	0,0063	0,6720	0,0318	0,6418	0,0060
	M1	-0,0095	0,0014	-0,0095	0,0007	0,0008	0,0019	0,0018	0,0004
	M2	0,0361	0,0049	0,0350	0,0061	0,2309	0,0173	0,2564	0,0070
	M3	0,0102	0,0007	0,0114	0,0003	0,0178	0,0012	0,0192	0,0005
	M4	0,0042	0,0005	0,0042	0,0006	0,0471	0,0048	0,0490	0,0017
	M5	-0,0121	0,0007	-0,0123	0,0007	0,0375	0,0047	0,0409	0,0045
	M6	0,0022	0,0001	0,0023	0,0001	-0,0007	0,0008	-0,0021	0,0004
a-Ketoglutarate_346	M0	0,9939	0,0014	0,9935	0,0009	0,8738	0,0057	0,8691	0,0084
	M1	-0,0042	0,0002	-0,0041	0,0000	0,0003	0,0007	0,0006	0,0008
	M2	0,0119	0,0015	0,0118	0,0015	0,0799	0,0043	0,0877	0,0047
	M3	0,0032	0,0002	0,0039	0,0006	0,0122	0,0007	0,0125	0,0005
	M4	-0,0053	0,0002	-0,0055	0,0000	0,0299	0,0007	0,0260	0,0022
	M5	0,0003	0,0000	0,0003	0,0000	0,0047	0,0009	0,0050	0,0002
Serine_390	M0	0,9232	0,0128	0,9356	0,0140	0,9507	0,0010	0,9492	0,0027
	M1	0,0154	0,0035	0,0118	0,0034	0,0068	0,0004	0,0073	0,0003
	M2	0,0113	0,0021	0,0087	0,0020	0,0069	0,0003	0,0070	0,0003
	M3	0,0505	0,0073	0,0444	0,0087	0,0360	0,0002	0,0369	0,0021
Alanine_260	M0	0,1440	0,0138	0,1814	0,0048	0,1767	0,0243	0,1712	0,0085
	M1	0,0035	0,0002	0,0030	0,0002	0,0041	0,0002	0,0041	0,0002
	M2	0,0280	0,0006	0,0270	0,0001	0,0274	0,0012	0,0274	0,0005
	M3	0,8285	0,0133	0,7924	0,0047	0,7953	0,0229	0,8007	0,0083

Supplemental Table 4. MID from [U-$^{13}C_5$]glutamine under hypoxia.

Metabolites	mass isotopomers	siCtrl		siCtrl+OSM		siHIF-1α		siHIF-1α+OSM	
		average	stdev	average	stdev	average	stdev	average	stdev
Malate_419	M0	0,1885	0,0033	0,2016	0,0066	0,1562	0,0000	0,1663	0,0016
	M1	0,0075	0,0001	0,0065	0,0005	0,0334	0,0038	0,0282	0,0008
	M2	0,0732	0,0020	0,0771	0,0026	0,1126	0,0058	0,1081	0,0002
	M3	0,3567	0,0098	0,3841	0,0024	0,2224	0,0019	0,2473	0,0026
	M4	0,3789	0,0087	0,3352	0,0071	0,4814	0,0077	0,4557	0,0038
Lactate_261	M0	0,9866	0,0019	0,9861	0,0000	0,9823	0,0005	0,9863	0,0009
	M1	0,0024	0,0003	0,0027	0,0002	0,0029	0,0004	0,0026	0,0002
	M2	0,0039	0,0002	0,0041	0,0000	0,0043	0,0001	0,0038	0,0001
	M3	0,0081	0,0005	0,0073	0,0002	0,0106	0,0008	0,0079	0,0001
Methionine_320	M0	1,0055	0,0008	1,0061	0,0005	1,0061	0,0002	1,0064	0,0009
	M1	-0,0032	0,0009	-0,0038	0,0006	-0,0043	0,0003	-0,0040	0,0008
	M2	-0,0009	0,0002	-0,0009	0,0002	-0,0006	0,0000	-0,0010	0,0001
	M3	-0,0006	0,0003	-0,0005	0,0001	-0,0003	0,0001	-0,0004	0,0000
	M4	-0,0001	0,0000	-0,0001	0,0001	-0,0002	0,0000	-0,0001	0,0000
	M5	-0,0009	0,0000	-0,0009	0,0000	-0,0009	0,0000	-0,0009	0,0000
Succinate_289	M0	0,4959	0,1199	0,4762	0,0069	0,5527	0,0313	0,4052	0,1895
	M1	-0,0023	0,0020	-0,0005	0,0007	0,0132	0,0027	0,0171	0,0075
	M2	0,0237	0,0054	0,0264	0,0021	0,0608	0,0080	0,0809	0,0285
	M3	0,0182	0,0031	0,0191	0,0002	0,0162	0,0008	0,0198	0,0040
	M4	0,4672	0,1098	0,4816	0,0103	0,3592	0,0195	0,4795	0,1508
Pyruvate_174	M0	0,9912	0,0008	0,9940	0,0019	0,9876	0,0002	0,9922	0,0013
	M1	-0,0026	0,0003	-0,0022	0,0004	-0,0015	0,0001	-0,0023	0,0004
	M2	0,0028	0,0001	0,0023	0,0005	0,0031	0,0000	0,0024	0,0001
	M3	0,0087	0,0002	0,0062	0,0019	0,0110	0,0006	0,0084	0,0001
Fumarate_287	M0	0,1173	0,0026	0,1296	0,0049	0,1477	0,0062	0,1474	0,0047
	M1	0,0884	0,0019	0,0977	0,0037	0,1113	0,0047	0,1111	0,0035
	M2	0,0834	0,0018	0,0922	0,0035	0,1050	0,0044	0,1048	0,0033
	M3	0,3350	0,0069	0,3662	0,0049	0,1963	0,0041	0,2235	0,0014
	M4	0,3770	0,0132	0,3144	0,0073	0,4409	0,0115	0,4144	0,0109
Glycine_246	M0	1,0000	0,0003	0,9998	0,0007	0,9998	0,0001	0,9984	0,0028
	M1	-0,0015	0,0004	-0,0011	0,0006	-0,0013	0,0000	-0,0011	0,0007
	M2	0,0019	0,0001	0,0017	0,0002	0,0018	0,0001	0,0030	0,0021
Glutamate_432	M0	0,0421	0,0039	0,0546	0,0150	0,0730	0,0001	0,0768	0,0007
	M1	0,0015	0,0002	0,0018	0,0004	0,0237	0,0032	0,0215	0,0001
	M2	0,0155	0,0006	0,0175	0,0018	0,0378	0,0025	0,0409	0,0010
	M3	0,0331	0,0008	0,0331	0,0022	0,1142	0,0080	0,1103	0,0009
	M4	0,0428	0,0012	0,0426	0,0005	0,0344	0,0015	0,0354	0,0011
	M5	0,8680	0,0052	0,8530	0,0204	0,7200	0,0123	0,7178	0,0029
Aspartate_418	M0	0,2402	0,0619	0,3776	0,1654	0,1535	0,0046	0,1731	0,0023
	M1	0,0085	0,0013	0,0054	0,0029	0,0356	0,0035	0,0314	0,0007
	M2	0,0696	0,0044	0,0609	0,0138	0,1155	0,0057	0,1111	0,0003
	M3	0,3272	0,0192	0,2934	0,0771	0,2141	0,0007	0,2318	0,0044
	M4	0,3585	0,0378	0,2658	0,0725	0,4863	0,0042	0,4575	0,0013
Citric acid_591	M0	0,0990	0,0125	0,1024	0,0044	0,1487	0,0087	0,1456	0,0096
	M1	0,0043	0,0005	0,0047	0,0001	0,0407	0,0055	0,0350	0,0015
	M2	0,0315	0,0009	0,0356	0,0022	0,0879	0,0068	0,0898	0,0025
	M3	0,0616	0,0007	0,0641	0,0026	0,1304	0,0058	0,1378	0,0049
	M4	0,0819	0,0010	0,0791	0,0011	0,2057	0,0046	0,2011	0,0053
	M5	0,7175	0,0127	0,7112	0,0089	0,3767	0,0139	0,3813	0,0017
	M6	0,0076	0,0007	0,0064	0,0016	0,0119	0,0000	0,0113	0,0000
a-Ketoglutarate_346	M0	0,0367	0,0006	0,0393	0,0043	0,0683	0,0000	0,0710	0,0017
	M1	0,0021	0,0001	0,0020	0,0001	0,0206	0,0031	0,0181	0,0005
	M2	0,0149	0,0005	0,0170	0,0018	0,0369	0,0023	0,0385	0,0004
	M3	0,0303	0,0009	0,0303	0,0023	0,1063	0,0083	0,1017	0,0018
	M4	0,0395	0,0005	0,0396	0,0006	0,0330	0,0010	0,0334	0,0000
	M5	0,8826	0,0007	0,8774	0,0091	0,7399	0,0127	0,7425	0,0012
Serine_390	M0	1,0039	0,0005	1,0040	0,0002	1,0034	0,0001	1,0036	0,0012
	M1	-0,0037	0,0004	-0,0037	0,0003	-0,0033	0,0001	-0,0033	0,0007
	M2	0,0000	0,0001	-0,0001	0,0000	0,0001	0,0000	0,0001	0,0006
	M3	-0,0002	0,0000	-0,0001	0,0000	-0,0002	0,0000	-0,0002	0,0001
Alanine_260	M0	0,9515	0,0051	0,9569	0,0105	0,9477	0,0027	0,9534	0,0013
	M1	-0,0025	0,0001	-0,0023	0,0001	-0,0005	0,0001	-0,0017	0,0002
	M2	0,0113	0,0010	0,0107	0,0021	0,0101	0,0003	0,0097	0,0004
	M3	0,0400	0,0043	0,0350	0,0083	0,0431	0,0023	0,0388	0,0007